Università Politecnica delle Marche

Dipartimento Scienze della Vita e Dell'ambiente

Doctoral Thesis in Biomolecular Sciences

Structural and aggregation properties of bovine α_1-acid glycoprotein, a member of the lipocalin superfamily

Candidate

Dr. Beatrice Maggiore

Supervisor

Prof. Fabio Tanfani

XV Cycle

2013 - 2016

ABSTRACT

α_1-Acidglycoprotein (AGP) is an important member of the acute phase response involved in drug binding and modulation of the immune system. AGP belongs to the lipocalin superfamily, a wide group of proteins sharing a strikingly conserved β-barrel fold that serves as a binding site for a large number of hydrophobic and neutral molecules. Several biological functions have been associated to AGP, both in *vivo* and in *vitro*. These include, among others, the ability to down-modulate the immune reaction upon insurgence of the acute phase response, thus acting as negative feedback control. Additionally, AGP is able to bind and transport a wide number of hydrophobic molecules. Binding is considered as a way to decrease the free concentration of a molecule. Potential therapeutic uses of AGP in the treatment of immune diseases have been envisioned, including, for instance, reduction of histamine levels. In the light of these observations, a detailed knowledge of the structure and stability of AGP appears essential.

Fourier-Transform infrared (FT-IR) spectroscopy has been extensively used in the investigation of AGP due to its sensitivity towards fluctuations within protein structures. Additionally, the technique is particularly well suited to study β-sheet-rich proteins. A survey of several environmental conditions, including pH and disulfide redox state, has shown that under reducing conditions, no molten globule state was observed, whilst strongly acidic and reducing environments induce concomitant denaturation and aggregation of the polypeptide chain following increases in temperature.

Further research has been undertaken to characterize AGP aggregates obtained in the presence of the disulfide-specific reducing agents. Transmission Electronic Microscopy analysis and binding of the Thioflavin T dye indicate that the aggregates possess a cross-β motif, suggesting that they are amyloid in nature. A molecular interpretation on the fibrillation kinetics of AGP was proposed. The experimental data do not show a nucleation-dependent polymerization mechanism otherwise they suggest a downhill polymerization mechanism as described for transthyretin and serum albumin. In this model, an aggregation-prone species self-assembles to form the amyloid fibrils. Further support to the downhill polymerization mechanism was provided by the seeding experiments and a more accurate kinetic analysis of fibril formation.

ESTRATTO IN LINGUA ITALIANA

Lo studio delle proprietà strutturali e funzionali della α_1-glicoproteina acida (AGP), nota anche come orosomucoide, costituisce l'oggetto di questa tesi. La AGP rappresenta, dopo l'albumina, la più abbondante proteina nel plasma, con concentrazioni fisiologiche comprese tra 0,5 e 1,5 mg/mL. Essa appartiene alla famiglia delle lipocaline, un ampio gruppo di proteine ubiquitarie accomunate da una struttura centrale a barile β (β-barrel) che funge da sito di legame per un elevato numero di molecole idrofobiche. Sono numerose le funzioni attribuite, sia in *vivo* che in *vitro*, all' AGP. Queste includono, tra le altre, la capacità di modulare negativamente l'attività del sistema immunitario in seguito all'insorgenza della risposta da fase acuta, e di legare/trasportare numerose molecole ad attività biologica. Il legame a tali molecole è da molti considerato come un modo per ridurne la concentrazione. Non sorprende, quindi, che l'AGP sia in grado di legare numerose citochine pro-infiammatorie, incluse quelle coinvolte nella sintesi e nel rilascio della stessa proteina. In virtù di tali proprietà, sono stati ipotizzati potenziali usi dell'AGP nella cura di disfunzioni del sistema immunitario, come nel ridurre i livelli di istamina durante uno shock anafilattico. Ne è stata, inoltre, dimostrata l'applicabilità biotecnologica nel campo dello sviluppo di nuovi biosensori, delle cromatografie e delle purificazioni industriali. Alla luce di tali considerazioni, l'ottenimento di informazioni dettagliate riguardo la struttura e la stabilità di questa proteina appare di primaria importanza. Gli studi effettuati sulla denaturazione termica dell'AGP in condizioni di pH neutro hanno evidenziato la presenza di un molten globule, un intermedio di folding nei processi di denaturazione di molte proteine. Il molten globule (letteralmente, globulo fuso), può essere considerato una forma più rilassata e flessibile della struttura terziaria di una proteina, in cui gli elementi di struttura secondaria risultano invariati o solo parzialmente destabilizzati. La spettroscopia IR con Trasformata di Fourier (FT-IR) è stata ampiamente utilizzata nello studio di molte proteine ricche di strutture β, in virtù della sua preferenzialità d'analisi per questo tipo di struttura secondaria e della sua sensibilità verso fluttuazioni strutturali dello scheletro polipeptidico. Durante il mio dottorato, è stata condotta un'analisi di ampio respiro riguardante numerosi fattori ambientali (pH, stato ossidoriduttivo, temperatura), la quale ha mostrato la presenza di intermedi strutturali di tipo molten globule, inoltre, valori di pH debolmente o fortemente acidi e/o condizioni riducenti, inducono la concomitante denaturazione e aggregazione delle catene polipeptidiche in seguito all'aumento della temperatura.

Un'ulteriore linea di ricerca percorsa durante il dottorato ha riguardato la caratterizzazione delle forme aggregate dell'AGP ottenute in specifiche condizioni di pH, temperatura e stato ossidativo dei ponti disolfurici. La capacità, di questi aggregati, di legare la Tioflavina T indica che tali forme aggregate sono di natura amiloide. L'analisi mediante microscopia elettronica in trasmissione (TEM) mostra che le fibrille amiloidi formatesi in condizioni riducenti sono abbondanti, lunghe e possiedono, numerosi punti di ramificazione. Indagini più mirate sono state condotte nello studiare la cinetica di formazione delle fibrille, da cui ricavare parametri cinetici utili nell'individuare un possibile modello di aggregazione. È importante notare che le analisi cinetiche non mostrano la presenza di una fase di nucleazione, il che esclude il modello di polimerizzazione dipendente da nucleazione. In questo modello, il passaggio limitante, è rappresentato dalla formazione di un nucleo che funge da innesco critico per l'intero processo di fibrillazione. Dati sperimentali hanno evidenziato la mancanza di questa fase, il che suggerisce un meccanismo a cascata, in cui lo step critico è rappresentato dalla conversione del monomero stabile in monomero 'attivato', il quale è più propenso all'aggregazione e si assembla in strutture fibrillari.

AIM OF THE WORK

The work presented in this thesis aims to shed new light on the structural and aggregation properties of bovine α_1-acid glycoprotein (bAGP). In particular:

- to investigate the role of pH and disulfide bridges redox state on the temperature-induced formation of aggregates in the denaturation pathway of bAGP.
- to investigate the nature of the aggregates formed by bAGP at different pH and in the absence or presence of a disulfide-specific reducing agent.
- to assess the possible molecular events responsible for conversion of the soluble monomer into aggregation-competent species.

LIST OF PUBLICATIONS

Paper I

Baldassarre M, Galeazzi R, **Maggiore B**, Tanfani F, Scirè. A
Bovine α1-acid glycoprotein, a thermostable version of its human counterpart: insights from Fourier transform infrared spectroscopy and in silico modelling.
Biochimie. 2014. 102: 19-28.

Paper II

Baldassarre M, **Maggiore B**, Scirè A, Tanfani F.
Amyloid fibril formation by bovine α1-acid glycoprotein in a reducing environment: The role of disulfide bridges on the observed aggregation kinetics.
Biochimie. 2015. 118: 244-52.

Publications not included in this thesis:

Paper III

Amabili P, Amici A, Civitavecchia A, **Maggiore B**, Orena M, Rinaldi S, Tolomelli A.
Highly stable atropisomers by electrophilic amination of a chiral γ-lactam within the synthesis of an elusive conformationally restricted analogue of α-methylhomoserine.
Amino Acids. 2016. 48(2): 461-78.

ABBREVIATIONS

AGP	α_1-Acid glycoprotein
bAGP	bovine α_1-Acid glycoprotein
DP	Downhill polymerization
FT-IR	Fourier Transform infrared
Hepes	4-(2-hydroxyethyl)-1-piperazineethanesulfonic acid
hAGP	human α_1-Acid glycoprotein
K_{agg}	Aggregation constant
K_i	Intermediate constant
MD	Molecular Dynamics
NDP	Nucleation-dependent polymerization
PDB	Protein Data Bank
TEM	Transmission electron microscope/microscopy
ThT	Thioflavin T

CONTENTS

1. BOVINE α_1-ACID GLYCOPROTEIN

This chapter provides a brief overview of the structural and functional properties of lipocalins superfamily in particular of the bovine α_1-acid glycoprotein (bAGP), the major subject explained in this thesis.

1.1 LIPOCALIN SUPERFAMILY

Members of the lipocalin protein superfamily are typically small extracellular proteins (160–180 residues in length), which are, perhaps, the best known for their binding to a remarkable range of small hydrophobic ligands. The structural features of the lipocalin fold are well adapted to the task of ligand binding: the amino acid composition of the pocket and loop scaffold, as well as its overall size and conformation, determine the selectivity. (1)
This large and diverse group of extracellular proteins are found in vertebrates and invertebrate animals, plants, and even in bacteria. This group and its name were originally proposed by Syed Pervaiz and Keith Brew. (2-4)
They include invertebrate colorant proteins, such as lobster crustacyanin, rodent pheromone transport proteins such as α_2-urinary globulin, various clinically important human plasma proteins (such as retinol-binding protein, α_1-acid glycoprotein, and α_1-microglobulin), ruminant milk β-lactoglobulin, the brain enzyme prostaglandin D synthase, as well as all important mammalian aeroallergens, and implicated in the regulation of the immune response as listed in Table 1. (5)
In spite of their initial classification only as ligand transport proteins, remarkably differing physiological roles were assigned to them, such as modulation of cell growth and metabolism (for Apolipoprotein D, NGAL (6)), regulation of the immune response (for AGP (6-8), α_1-Microglobulin (9), GLY, Complement factor 8 γ chain), enzymatic synthesis of prostaglandin D2, retinol transport (for RBP) and, furthermore, a role in olfaction (for Odorant-binding protein). (10)
In the last few years, based on these diverse functions, the lipocalins have found medical application as diagnostic indicators, for instance AGP and NGAL as inflammation markers in mammals (11, 6), α_1m as the major urinary marker of renal disorders (9), and GLY as a pregnancy marker. (12)
Furthermore, lipocalins from bloodsucking insects have evolved as scavengers for mediators of inflammation. As well as using the natural ligand-binding function, lipocalins have potential applications as antidotes, antagonistic protein therapeutics or as target-recognition modules in a new generation of immunotoxins. (7)

Name	Common abbreviation	Alternative names and acronyms
Bacterial lipocalin	Blc	
Extracellular fatty acid-binding protein	Ex-FABP	chondrocyte 21 protein (Ch21), P20K, quiescence-specific protein (QSP)
Retinol-binding protein	RBP	plasma retinol-binding protein, serum retinol-binding protein (sRBP)
β-Lactoglobulin	βlg	βLac, BLG
	Glc	pregnancy protein 14 (PP14), human pregnancy-

Glycodelin		associated endometrial protein, α_2-globulin (α_2-PEG), chorionic α_2-microglobulin, progestagen-associated endometrial protein (PAEP), α-uterine protein
α_1-Acid glycoprotein	AGP	orosomucoid (ORM), seromucoid α_1 fraction, α_1-S
α_1-Microglobulin	A1M	α_1-m, α_1m, protein HC, α_1-microglycoprotein
Apolipoprotein D	apoD	gross cystic disease fluid protein (GCDFP-24), apocrine secretion odour-binding protein (ASOB-2)
Complement factor 8 γ chain	C8γ	C8G
α_{2u}-Globulin	α_{2u}	rat α_2-urinary globulin, mouse major urinary protein (MUP)
Odorant-binding protein	OBP	frog Bowman's gland protein
Allergens		
Mouse urine allergen	Mus m 1	MUP
Major cow dander allergen	Bos d 2	bovine dander allergen (BDA20)

Table 1.1. Names, abbreviations, acronyms and alternative names for some members of the lipocalin superfamily. Table adapted from Bo Åkerstrom et al. 2000. (5, 13)

1.2 STRUCTURE OF BOVINE α_1-ACID GLYCOPROTEIN

Lipocalins demonstrate usually good levels of sequence similarity even though they share one to three short, conserved sequence motifs. The existence of the lipocalin superfamily is proved by a conserved folding pattern common to all lipocalin structures determined to high resolution by X-ray crystallography. (14) The lipocalins were initially defined according to amino acid sequence similarity. A protein 'family' gathers molecules whose sequence similarity is high enough (typically 35% or more) to demonstrate a common ancestry whereas a 'superfamily' is included of proteins whose shared origin is verified, typically by clear structural relationship, despite their low sequence similarity. Lipocalins structure are highly conserved and are composed of a single eight-stranded continuously hydrogen-bonded antiparallel β-barrel, which encloses an internal ligand-binding site. Although it is seems to be a general relationship among the eukaryotic lipocalins at the level of gene structure (15-17) as well as intron/exon organization (18) the human lipocalins simply show weak sequence similarity. However, all of them share a common three-dimensional structure with a conserved β-barrel architecture. (14, 19)
Human AGP (hAGP) shows the typical lipocalin fold, composed of a central 8-stranded,antiparallel β-barrel flanked by an α-helix. (20) The protein contains two disulfide bridges, the importance of which has been investigated. (21-23)
Bovine α_1-acid glycoprotein (bAGP) also called orosomucoid belongs to the lipocalins superfamily (20): AGP has been further classified in a subset of lipocalins, the so called "immunocalins", a subfamily of proteins that may also immunomodulate the inflammatory reaction. (24)
The research performed during my doctoral studies has been directed towards a better understanding the structure and functions of bovine α_1-acid glycoprotein.

Bovine AGP (bAGP) is a glycoprotein of 42 kDa, as determined by SDS-PAGE, the carbohydrate moiety accounting for 26.6% of its molecular weight. (25) More recently, the molecular weight of bAGP was fixed to 33.8 kDa by MALDI-TOF mass spectrometry analysis. (26) Under physiological conditions, bAGP has a stable, high-serum concentration of ~1 g l^{-1}.
In Figure 1.1B, the proposed bAGP model structure reveals a typical lipocalin fold comprising an eight-stranded β-barrel (strands A–H as in Figure 1A) as a central folding motif, which is flanked by α-helixs. As in other proteins of this family, such as the retinol binding protein (PDB ID: 1RBP), apolipoprotein D (PDB ID: 2APD) and β-lactoglobulin (PDBID:1BEB), four loops connecting the β-strands form the entrance to a ligand pocket at the open end of the barrel. (20,27) The C-terminal segment of bAGP ends in an α-helix with approximately two turns. The closed end of the β-barrel is covered by the N-terminal 3_{10}-helix. Both termini of the polypeptide chain are covalently attached to the β-barrel via two disulphide bridges (Cys5–Cys148 and Cys73–Cys166); another free cysteine (Cys59) protrudes from the barrel towards the solvent. These disulphide bridges are a recurring feature of several other lipocalins from different species. (28) Three of the four N-glycosylation sites (Asn39, Asn76 and Asn86) are located at the closed end of the β-barrel. (29) The glycan chain at Asn118 (loop 7), lines the entrance to the ligand pocket of bAGP and, according to the authors, may alter its shape and ligand selectivity.

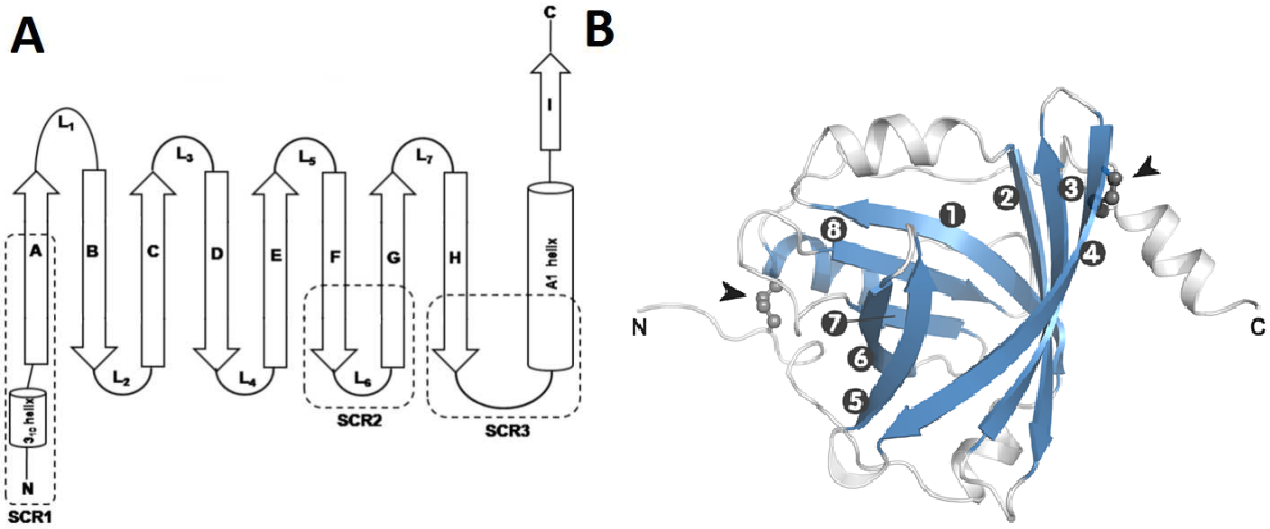

Figure 1.1. The conserved lipocalin fold. (A): The strands [A-I] of the β-sheet and the helices are represented as arrows and cylinders respectively. The loops connecting the strands are marked as L1-L7. The three Structurally Conserved Regions (SCR) are marked as SCR1, SCR2 and SCR3 respectively. (15)
(B): Proposed model structure of bAGP: 3D secondary structure elements making up the typical lipocalin fold. β-strands are labelled 1-8. Arrowheads denote the disulfide bridges. (29)

bAGP is mainly synthesized in the liver, but it can be produced in several other tissues. The extrahepatic expression of bAGP has been detected especially in mammary glands, salivary glands and spleen. (30-32) From these findings, it has been postulated that bAGP may play its immunomodulatory role also during inflammatory threats in the mammary gland, in exocrine gland ductal systems, in saliva and enteric mucosa. (30-32)
Until today, detailed structural information on bAGP refer only to the carbohydrate chains, (33, 34) showing that bAGP exhibits unique sialic acid-containing oligosaccharides composed of only N-glycolylneuraminic acid. (26) Very little is known on the structure and stability properties of the protein, as no experimental structures are available.

1.3 BIOLOGICAL FUNCTIONS: DRUG BINDING

Together with serum albumin and lipoprotein, AGP represent the most important drug binder and carrier, directly affecting the pharmacodynamics and pharmacokinetics of several drugs. Alterations in the plasmatic levels of AGP during the APR and other pathological conditions influence the concentration of free drugs, even though the total drug concentration remains unchanged. Due to the architecture of its binding site and to the overall chemical/physical properties of this protein, AGP mostly binds neutral or basic drugs displaying significant hydrophobicity. (35) Ligands can be of exogenous origin, such as tamoxifen, (36) propanol, (37) coumarin (38) and chlorpromazine (39) or endogenous biomolecules natively present in our bodies, such as serotonin, platelet activating factor (PAF), (40) melatonin, (41) histamine (42) and progesterone. (39) Although acidic drugs are mostly bound and carried by serum albumin, exceptions have been reported, including retinoic acid (RA) and phenobarbital. (43) This is particularly true when the levels of bAGP increase, or when those of albumin decrease, which is commonly the case during the acute phase response. (44) Although the binding of drugs has been reported to be mostly hydrophobic in nature, several studies also point to the existence of electrostatic interactions. This may also explain the observed increase in binding capacity at high pH value, that can be explained by the increased net charge difference between the negatively-charged protein and the positively charged drugs. (45)

1.4 BIOLOGICAL FUNCTIONS: IMMUNOMODULATORY PROPERTIES

α_1-acid glycoprotein has been shown to exert modulating actions on several cell types of the immune system. (46, 47) It has been proposed, and it is widely accepted nowadays, that bAGP acts primarily as a feedback down-regulator of the immune response in several of pathological conditions. This action allows for a progressive attenuation of the body's state of alert, restoring homeostasis and preventing side-effects caused by "triggered" defence mechanisms. Direct effects on several different cell types have been described both in vitro and in vivo. In vitro, AGP is able to prevent activation of neutrophils (47, 48) and to inhibit their typical activated immune responses, such as chemotactic extravasation and generation of reactive oxygen species (ROS).(47) Additionally, it prevents platelet aggregation by decreasing the local concentration of PAF.(48) This has been shown to be particularly efficient towards the second wave of platelet recruitment, when more platelets are massively recruited from the bloodstream to the site of infection or lesion and are activated by chemical signals produced by the cells already present. (49)

AGP has an anti-proliferative effect on T-lymphocytes. (50) The precise mode of action remains elusive, but interaction between the glycan moiety and the cell membrane seems to be essential, possible leading to activation of the protein tyrosine kinase pathway. (51) Enhanced inhibition is showed by highly- branched AGP glycoforms, while desialylated (asialo) glycoforms display a reduced inhibitory potential. The latter feature is in contrast with the increased inhibition of platelets observed upon desialylation. The key role of glycans in the T-cell inhibition properties has been demonstrated by experiments in which a synthetic carrier conjugated with the oligosaccharides obtained from AGP showed comparable inhibition with respect to native AGP. (52)

Further mechanisms by which bAGP counteracts the immune response involve adhesion inhibition of several leukocytes (such as neutrophils, monocytes, T lymphocytes and macrophages) to

endothelial cells or aggregated platelets in close proximity of the inflamed areas. These express E-selectins, carbohydrate-binding protein protruding from the cell membrane that are able to bind sialic acid containing glycoproteins expressed by leukocytes, such as the E-selectin ligand-1 (ESL-1). It has been shown that AGP is recognised by E-selectins. (53) Consequently, rolling, adhesion and extravasation of leukocytes may then be inhibited. It has been proposed that AGP in a non-specific anti-infectious agent. This function could be due to the high amount of sialic acid residues, which are typically found associated with sialo membrane proteins. (54) AGP could therefore function as a non-specific competitor for cell surfaces, blocking the binding and the invasion of infective agents in a similar way to what has been observed with leukocytes. It has been observed that AGP inhibits the ability of Plasmodium falciparum to infect red blood cells. On the other hand, AGP can also inhibit the attachment and subsequent internalization of Mycoplasma pneumoniae by human alveolar macrophages (55) thus acting as an inhibitor of phagocytosis.

2. MATERIALS AND METHODS

2.1 INFRARED SPECTROSCOPY

Infrared (IR) spectroscopy is a powerful biophysic tool for protein investigations. It makes up, together with Raman and vibrational Circular Dichroism (CD), the family of vibrational spectroscopies. As the name implies, vibrations of atoms, functional groups or molecules as a whole are the observed phenomenon. This chapter aims to provide illustrative explanations to help understand the fundamentals of infrared spectroscopy and how infrared radiation and matter interact with each other.

2.1.1 APPLICATIONS AND ADVANTAGES

Biological IR spectroscopy since its advent in the beginner of the 20th century, has been applied to characterize and investigate many types of molecules important for life such as DNA, lipids, protein and even living cells and tissues. (56) One of the great advantages of IR spectroscopy is its versatility, it is valid to all systems ranging for small soluble proteins to large membrane protein and even insoluble aggregates. (57)

2.1.2 THE ELECTROMAGNETIC SPECTRUM

Maxwell's classical theory of electromagnetic radiation considers electromagnetic radiation as electric and magnetic fields oscillating in single planes at a right angle to each other.

These fields are characterized by their wavelength λ and frequency υ. Frequency is described as the number of waves that pass a given point in a unit of time and wavelength is the distance from a maximum of one wave to the crest of the adjacent wave. There are two values related by following equation

$$v = c/\lambda \tag{2.1}$$

where *c* is the speed of light.

In vibrational spectroscopy, it is more common use another unit: the wavenumber ($\bar{\upsilon}$) which is defined by the number of wave in a length of one centimeter and is given by the following relationship:

$$\bar{\upsilon} = \frac{1}{\lambda} = \frac{\upsilon}{c} \tag{2.2}$$

Wavenumber is the reciprocal of the wavelength, which has the advantage of being proportional to the energy ($E = h\upsilon$). The unit of wavenumber is cm^{-1}. The range of the electromagnetic spectrum and the relations between wavelength, wavenumber and energy are shown in Figure 2.1

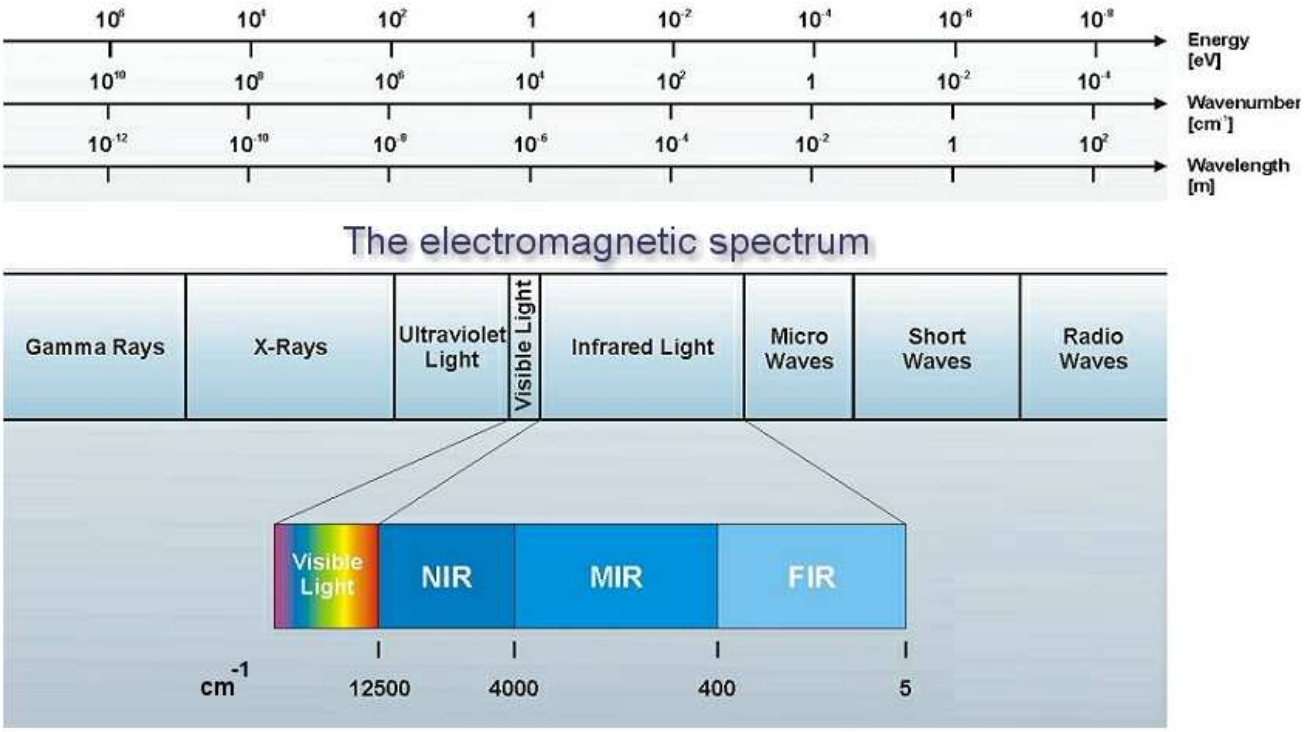

Figure 2.1. The wavelength ranges of the electromagnetic spectrum. Energy is proportional to wavenumber, but inversely proportional to wavelength

Wavelengths associated with infrared radiation are commonly considered as those ranging from the lower edge of red light (750 nm or ~13,000 cm^{-1}) to the upper edge or microwaves (1 mm or 10 cm^{-1}). This interval is conveniently divided into NIR, Near Infrared Region (~12,500–4,000 cm^{-1}), MIR, Mid Infrared Region (~4,000–400 cm^{-1}) and FIR, Far Infrared Region (~400–5 cm^{-1}), as described in Figure 2.1. Nevertheless, the mid infrared is the spectral region where most biological systems are investigated and all infrared measurements described in this thesis have been performed in this region.

2.1.3 INTERACTION WITH MATTER: MOLECULAR VIBRATION

During the late 19th century-beginning of 20th century it was proposed that the electromagnetic radiation can be considered as a stream of particles called photons. Each photon contains a defined amount of energy given by the Bohr equation:

$$E = h\upsilon \tag{2.3}$$

where h is the Planck constant and υ is the equivalent of the classical frequency (Eq 2.1).

Most of the vibrational energies within the molecule fall into the infrared region of the electromagnetic spectrum. Vibrational energy of a molecule is described by its vibrational frequency.

Infrared spectroscopy is based on the absorption of infrared light by the substance to be measured.

The following simple model of harmonic oscillator used in classical physics describes infrared absorption. If atoms are considered to be particles with a given mass, then the vibrations in a dynamic molecule can be describe as follows:

if one considers the simple case of a molecule made up of two oscillating atoms joined by a spring/bond, then the vibrational frequency of such a bond can be described by the Hooke's law:

$$F = -k\Delta R \tag{2.4}$$

The frequency of oscillation is given by:

$$\upsilon = \frac{1}{2\pi}\sqrt{\frac{k}{\mu}} \tag{2.5}$$

where υ is vibrational frequency, k is the classical force constant and μ the reduced mass ($1/m_2 = 1/m_1 + 1/m_2$) of two atoms. This means that the frequency increases if the strength of the bond increases, or if the masses of the vibrating atoms decrease. (58)

The frequency of oscillation will, however, be unperturbed, since it only depends on the type of bond and masses of the two atoms. The introduction provided above explains the behavior of a di-atomic molecule. In these molecules, the only vibration is thus the stretching of the covalent bond. Most molecules, however, contain more that two atoms, so that several types of vibrations exist. Bonds in molecules or functional groups consisting of 3 atoms can also stretch in phase (symmetrical stretching) or out of phase (antisymmetrical stretching). Changes in bond angles are collectively referred to as bending vibrations and, according to the number of bonds and how the angles between them change, can be further classified into scissoring and rocking vibrations. (59) Figure 2.1 provides a graphical understanding of these motions, using a generic four- atom molecule as an example. Usually, bond length and angle oscillations can couple to one another, giving rise to the so called normal modes of vibration. Some normal modes localize on single functional groups (group vibrations), or extend across the whole molecule (skeletal vibrations). The latter give to rise complex band patterns, usually below 1500 cm^{-1}, that are hardly decipherable because they are unique to any given molecule. This is usually referred to as fingerprint region.

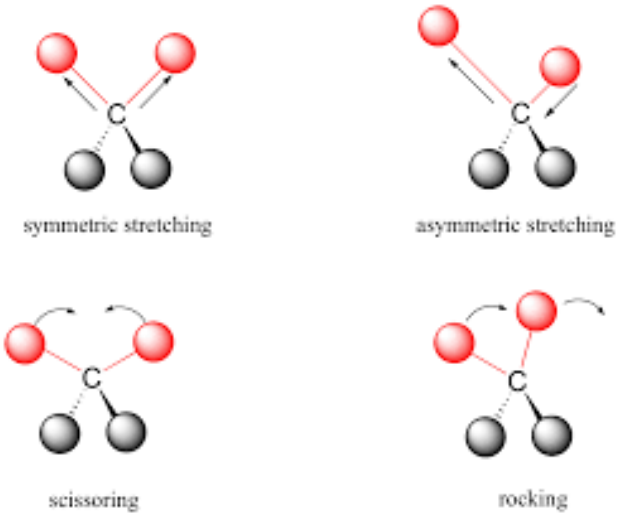

Figure 2.2. Typical vibrations occurring in a four-atom molecule. Arrows denote stretching or in plane bending of bond lengths and angles.

2.1.4 VIBRATIONS OF PROTEINS

Infrared spectroscopy provides information about the secondary and tertiary structure content. The most important group for the analysis of a peptide/protein is the peptide group, which has nine amide vibrations: A, B and I-VII. However, for the conformational analysis of the polypeptides only Amide I and Amide II vibrations modes are used.

Band	Approximate pos. (cm^{-1})	Composition
Amide A	3300	NH_s
Amide B	3100	NH_s
Amide I	1700–1600	CO_s (80%), CN_s, CCN
Amide II	1575–1480	NH_b (60%), CN_s (40%)
Amide III	1300–1230	CN_s (40%), NH_b (30%), CC_s (20%), CNC_d
Amide IV	760–625	CO_b^{oop} (40%), CC_s (30%), CNC_d
Amide V	800–640	NH_b^{oop}, CN_t
Amide VI	600–540	CO_b^{oop}, CN_t
Amide VII	200	NH_b^{oop}, CN_t, CO_b^{oop}

Table 2.1. Name, approximate position and composition of the nine amide vibrations in H_2O. Subscripts: s, stretching; b, bending; d, deformation; t, torsion. Superscript: oop, out-of- plane

The Amide I (1700-1600 cm^{-1}) mode originates mainly from the stretching vibration of the C=O bonds and to some extent from the stretching vibration of the C-N bonds. This vibration is highly sensitive to the conformation of the polypeptide backbone and therefore can be used to quantify the secondary structure content of the protein. The common band assignments for the secondary structure are presented in Table 2.3 below.

Secondary structure	Band position in H_2O	
	Average band position	Range
α-helix	1654	1648-1657
β-sheet	1633 1684	1623-1641 1674-1695
Random coil	1647	1642-1652
Turns	1672	1662-1686

Table 2.2. Assignment of amide I band positions of the secondary structure motifs. (60)

In certain cases it is seven possible to distinguish between parallel and antiparallel β-sheets. As show in Table 2.3 β-sheet have two bands in the region between 1600 and 1700 cm^{-1}. It has been shown that the high wavenumber band (1690 cm^{-1}) appears for planar antiparallel β-sheets with large number of strands, but not for small or twisted antiparallel β-sheets. It is also weak or not observable for the parallel β-sheet. (61, 62)

The Amide II (1600-1500 cm^{-1}) band arises mainly from the bending vibration of the N-H bond, as described in Table 2.1. Although it is sensitive to the backbone conformation, the correlation with the secondary structure content is less evident than in the amide I region. (60)

Water plays an important role in all biological processes. In the mid-IR range it has two main bands: a broad band around 3400 cm^{-1}, due to the stretching vibrations of the O-H group and a narrow band at 1640 cm^{-1}, due to the bending vibration of the O-H group. The latter band overlaps with the amide I band of the protein, which causes a severe problem in the interpretation of the spectra, thus many protein experiments are performed in ^2H_2O instead, which shifts the water absorption away from the amide I region (Figure 2.3). (63-65)

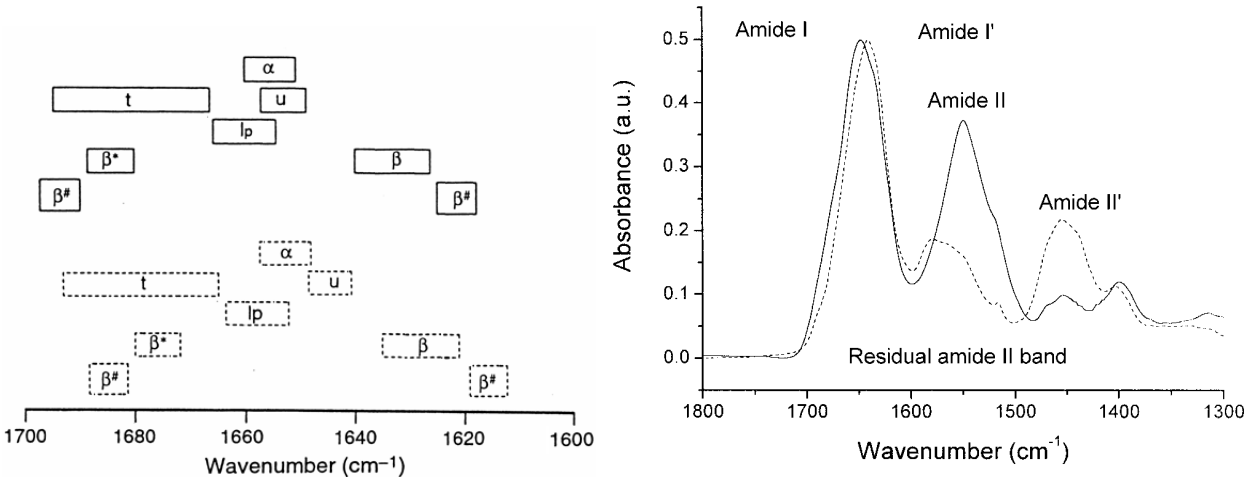

Figure 2.2. (Left Panel) The regions Amide I/I' (1600-1700 cm^{-1}) frequencies for protein secondary structures. Amide I (in H_2O): solid line frames; amide I' (in ^2H_2O): dashed line frames. (Right Panel) The infrared absorption spectra in Amide I/I' and Amide II/II' in H_2O (solid line) and in ^2H_2O (dashed line). (66)

2.2 FLUORESCENCE SPECTROSCOPY

Fluorescent probes enable researchers to detect particular components of complex biomolecular assemblies, with exquisite sensitivity and selectivity. The fluorescence process is the result of a process that occurs in certain molecules (generally polyaromatic hydrocarbons or heterocycles) called fluorophores or fluorescent dyes. A fluorescent probe is a fluorophore designed to respond to a specific stimulus or to localize within a specific region of a biological specimen.

2.2.1 PHOTOCHEMISTRY

Luminescence occurs when an orbital electron of a molecule, atom or nanostructure, relaxes to its ground state by emitting a photon of light after being excited to a higher quantum state by some type of energy. Fluorescence is the emission of light by a substance that has absorbed light or other electromagnetic radiation. (67)

Excitation:

$$S_0 + h\upsilon_{ex} \rightarrow S_1 \tag{2.6}$$

Fluorescence (emission):

$$S_1 \rightarrow S_0 + h\upsilon_{em} + heat \tag{2.7}$$

here $h\upsilon$ is a generic term for photon energy with (as introduced in eq. 2.3) h = Planck's constant and υ = frequency of light, (The specific frequencies of exciting and emitted light are dependent on the particular system).

The process responsible for the fluorescence of fluorescent probes and other fluorophores is illustrated by the simple electronic-state diagram (Jablonski diagram) shown in Figure 2.4.

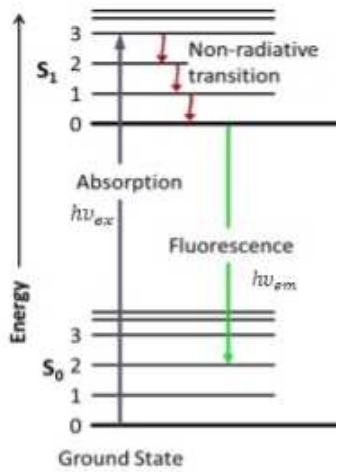

Figure 2.4. Jablonski diagram describes most of the relaxation mechanisms for excited state molecules. After an electron absorbs a high energy photon the system is excited electronically and vibrationally. The system relaxes vibrationally, and eventually fluoresces at a longer wavelength.

State S_0 is called the ground state of the fluorophore (fluorescent molecule) and S_1 is its first (electronically) excited state, exists for a finite time (typically 1–10 nanoseconds). A molecule, S_1, can relax by various competing pathways. It can undergo 'non-radiative relaxation' in which the excitation energy is dissipated as heat (vibrations) to the solvent. Excited organic molecules can also relax via conversion to a triplet state, which may subsequently relax via phosphorescence or by a secondary non-radiative relaxation step.

2.2.2 QUANTUM YIELD

The fluorescence quantum yield gives the efficiency of the fluorescence process. It is defined as the ratio of the number of photons emitted to the number of photons absorbed. (68,69)

$$\phi = \frac{number\ of\ photons\ emitted}{number\ of\ photons\ absorbed} \tag{2.8}$$

The maximum fluorescence quantum yield is 1.0 (100%); every photon absorbed results in a photon emitted. Compounds with quantum yields of 0.10 are still considered quite fluorescent. Another way to define the quantum yield of fluorescence, is by the rate of excited state decay:

$$\phi = \frac{K_f}{\sum K_i} \tag{2.9}$$

where K_f is the rate of spontaneous emission of radiation and $\sum K_i$ is the sum of all rates of excited state decay. Other rates of excited state decay are caused by mechanisms other than photon emission and are, therefore, often called "non-radiative rates", which can include: dynamic collisional quenching, near-field dipole-dipole interaction (or resonance energy transfer), internal conversion, and intersystem crossing. Thus, if the rate of any pathway changes, both the excited state lifetime and the fluorescence quantum yield will be affected.

2.2.3 STOKES SHIFT

In general, emitted fluorescent light has a longer wavelength and lower energy than the absorbed light. (70) This phenomenon, known as Stokes shift, is due to energy loss between the time a photon is absorbed and when it is emitted. The causes and magnitude of Stokes shift can be complex and are dependent on the fluorophore and its environment. However, there are some common causes. It is frequently due to non-radiative decay to the lowest vibrational energy level of the excited state. Another factor is that the emission of fluorescence frequently leaves a fluorophore in a higher vibrational level of the ground state.

2.2.4 FLUORESCENCE SPECTRA

For polyatomic molecules in solution, the discrete electronic transitions represented by $h\upsilon_{ex}$ and $h\upsilon_{em}$ in Figure 2.4 are replaced by rather broad energy spectra called the fluorescence excitation spectrum and fluorescence emission spectrum, respectively (Figure 2.5).

The absorption of energy to produce the first excited state does not perturb the shape of the molecule greatly and this means that the distribution of vibrational levels is very similar in both the ground and first excited states. The energy differences between the bands in the emission spectrum will be similar to those in the absorption spectrum and frequently the emission spectrum will be approximate to a mirror image of the absorption spectrum. Since the emission of fluorescence always takes place from the lowest vibrational level of the first excited state, the shape of the emission spectrum is always the same, despite changing the wavelength of exciting light

A plot of emission against wavelength for any given excitation wavelength is known as the emission spectrum. If the wavelength of the exciting light is changed and the emission from the sample plotted against the wavelength of exciting light, the result is known as the excitation spectrum.

The quantum efficiency of most complex molecules is independent of the wavelength of exciting light and the emission will be directly related to the molecular extinction coefficient of the compound.

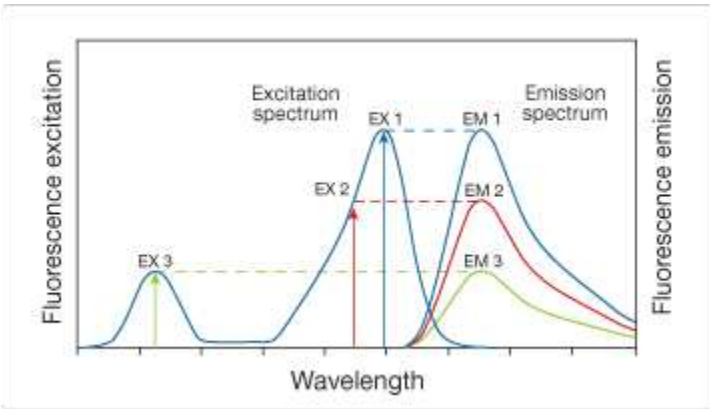

Figure 2.5. Excitation of a fluorophore at three different wavelengths (EX 1, EX 2, EX 3) does not change the emission profile but does produce variations in fluorescence emission intensity (EM 1, EM 2, EM 3) that correspond to the amplitude of the excitation spectrum.

2.3 MATERIALS

The following chemicals were purchased from Sigma-Aldrich: deuterium oxide (99.9 % ^2H_2O), ^2HCl, NaO^2H, TCEP-HCl, Hepes, piperazine, Thioflavin T. All other chemicals were commercial samples of the purest quality. Human and bovine α_1-acid glycoprotein from pooled plasma samples were purchased from Sigma and used without further purification.

2.3.1 PREPARATION OF SAMPLES FOR IR MEASUREMENTS

The following buffers were prepared for infrared measurements: 25 mM sodium citrate/^2HCl, p^2H 2.9 (buffer A); 50 mM piperazine/^2HCl, p^2H 4.5 (buffer B); 50 mM piperazine/^2HCl, p^2H 5.5 (buffer C); 50 mM Hepes/NaO^2H, p^2H 7.4 (buffer D). TCEP or DTT (5 mM) were present to the buffers described above if reducing conditions were needed. The p^2H value was measured with a standard pH electrode, and the value was corrected according to the following equation: $p^2H = pH + 0.4$. Lyophilised human and bovine AGP samples (~1.5 mg) were resuspended in 250 µL of the chosen appropriate buffer and briefly vortexed until the solution appeared clear by visual inspection. The protein samples were concentrated to ~20 µL by means of Amicon Ultra 0.5-mL (MWCO: 30 kDa) centrifugal filter devices (Millipore, Tullagreen, IRL) spunat 6800×g for 1h on an Allegra X-22 Rcentrifuge (Beckman Coulter). All samples were maintained at 4 °C throughout the centrifugation. Another 250 µL of buffer were directly added to the retentate, followed by an additional centrifugation step. This procedure was repeated several times to completely hydrate the protein molecules in the chosen deuterated buffer and to dilute out contaminating, protein-bound water molecules that may interfere with the IR analyses. The concentrated protein samples had typical volumes of ~20–40 µL and concentrations of ~3–5 % and were immediately subjected to IR measurements.

2.3.2 ACQUISITION AND ANALYSIS OF IR SPECTRA

The concentrated protein samples were injected into a thermostated Graseby Specac 20500 cell (Graseby-Specac Ltd., Orpington, Kent, U.K.) fitted with CaF_2 windows separated by a 25 µL Teflon spacer. FT-IR spectra were recorded by means of a Perkin-Elmer 1760-X Fourier transform infrared spectrometer using a deuterated triglycine sulphate (DTGS) detector and a normal Beer-Norton apodization function. During data acquisition, the spectrometer was continuously purged with CO_2-free dry air at a dew point of –70°C, generated by a Parker Balston 75-62 FT-IR air dryer (Balston AGS, Haverhill, MA). In thermal unfolding experiments, an external bath circulator (HAAKE F3) was used and spectra were collected every 5 °C in the 20–95 °C temperature range. The actual temperature in the cell was controlled by a thermo couple placed directly on to the windows. Spectra of buffers and samples were acquir data resolution of 2 cm^{-1} under the same scanning and temperature conditions. Spectra were collected and processed using the SPECTRUM software from Perkin-Elmer. Correct subtraction of H_2O was judged to yield an approximately flat baseline between 1900 and 1400 cm^{-1}, while subtraction of ^2H_2O was adjusted to the removal of the ^2H_2O bending absorption close to 1220 cm^{-1}. Deconvoluted parameters were set with a γ value of 2.5 and a smoothing length of 60 points. Second derivative spectra were calculated over a 13 data

point range (12 cm^{-1}). Difference spectra were obtained by subtracting the spectrum recorded at the lower temperature from the one recorded a temperature 5° C higher.

2.3.3 PREPARATION OF SAMPLES FOR FIBRILLATION KINETICS WITH THIOFLAVIN T

Stock human or bovine AGP solutions at various concentrations were prepared by dissolving the lyophilised proteins in 10 mM Hepes/NaOH, pH 7.4, to a final concentration of 10 mg/mL. The fibrillation kinetics of bAGP were obtained by monitoring the fluorescence emission of the bAGP/ThT complex (71-73) at pH 4.5 and 5.5 under reducing conditions by using 5mM TCEP or DTT as reductants.
Additional fibrillation kinetic experiments were carried out on pre-reduced bAGP (PR-bAGP) in the presence of TCEP or DTT. Pre-reduced bAGP was obtained by diluting aliquots of the bAGP stock solution with equal volumes of 10 mM Hepes/NaOH, 10 mM TCEP or 10 mM DTT, pH 7.4. The samples were incubated on a thermostated tube plate (Thermo Twister Comfort, Quantifoil Instruments GmbH, Jena, Germany) kept at an orbital shaking speed of 500 rpm. The reduction was allowed to proceed for 1 h at 65 °C. Under these conditions, the protein is destabilized, and not prone to aggregate.
Aliquots of appropriate volumes were withdrawn from each sample prior to incubation at the desired temperature in order to be used as control samples in subsequent analyses.

2.3.4 THIOFLAVIN T SPECTROSCOPIC ASSAY

Fibrillation buffers were transferred in to quartz cuvettes and let to equilibrate at the desired running temperatures for 30 minutes in the spectrofluorimeter thermostated cell holder equipped with an internal stirrer. To achieve thermal and compositional homogeneity before and during the measurements, a small stirring bar was applied to the reaction assay. The fibrillation reaction was started by addition of adequate amounts of unreduced or pre-reduced bAGP to the pre-equilibrated buffer. The fluorescence was recorded every 5 minutes for 24 hours by means of a Perkin-Elmer LS-50b spectrofluorimeter. In order to prevent photobleaching of ThT, the instrument was programmed to switch on the lamp every 5 minutes, to average the signal for 10 seconds and then to switch off the lamp. Acquisitions parameters were as follows: 440 nm excitation (5 nm slits), 482 nm emission (10 nm slits). All values were corrected by subtracting the emission intensity of the control samples. The corrected emission intensities were plotted versus the corresponding incubation time and fitted to a first order exponential decay function using OriginPro 7.5 software (OriginLab, Northampton, MA).

2.3.5 TRANSMISSION ELECTRON MICROSCOPY

The 6 h-treated AGP solutions were diluted to 0.5 or 1 mg/mL and then a 2 µL drop of the diluted solution was placed onto carbon-coated 300-mesh copper grids. Occasionally, the samples incubated for 30 or 48 h were also examined. The samples were left to adsorb for 10 min. Excess solution was removed by blotting with a small piece of filter paper placed on the border of the grids. The samples were stained with a 2 µL drop of 0.25% (w/v) lead citrate solution for 3 min. Excess stain was removed with a piece of filter paper and the grids were gently washed three times with 2 µL distilled water and then left to dry off. (74) The samples were examined on a Philips 208 transmission electron microscope at an accelerating voltage of 80 kV.

2.3.6 SEEDING

For the seeding trials, stock bAGP solutions were let to fibrillate in the presence of seeds for 24 hours at pH 5.5 in the presence of 5 mM DTT, 51 °C, or at pH 4.5 in the presence of 5 mM TCEP, 32 °C. A further seeding experiment was carried-out on PR-bAGP at pH 5.5, 5 mM TCEP, 40 °C. Seeds were produced by sonicating aliquots of fibrillated AGP in a Bransonic 1510E-MTH ultrasonic bath cleaner (Branson ultrasonics corporation, Danbury, USA). Sonication was performed at room temperature in 1.5 mL tubes containing 1 mL of sample, alternating 1 min sonication to 1 min pause for an overall sonication time of 3 min (75). The seeds (5 or 10% with respect to the total protein concentration) were immediately added to monomeric solutions of bAGP or PR-bAGP, and the fibrillation was monitored as described above.

3. RESULT AND DISCUSSION: THERMAL UNFOLDING PATHWAY OF BOVINE AGP

Until today, detailed structural information on bAGP refer only to the carbohydrate chains (34) showing that this protein exhibits unique sialic acid-containing oligosaccharides composed of only N-glycolylneuraminic acid. (26) Very little is known on the structure and stability properties of the protein, as no experimental structures are available.
In the Paper I the structure and the stability of bAGP has been investigated by FT-IR spectroscopy. The spectroscopic data revealed that bAGP features a significantly higher thermostability than its human counterpart, despite sharing a very similar structure.
The experimental data, further, confirm the pivotal role of disulfide bridges in the stability of bAGP, analogously to other lipocalins. (76, 29)

3.1 INFRARED ABSORPTION OF BOVINE AGP UNDER NATIVE CONDITIONS

The infrared absorption spectrum of bAGP was recorded under native conditions (pH 7.4, 20°C).
It shows two broad bands centered around 1630 and 1550 cm^{-1}, corresponding to the amide I and amide II modes, respectively (Figure 3.1 B, dashed lines). The infrared spectrum of the same sample prepared in deuterated buffer and recorded under the same experimental conditions shows peculiar differences. The amide I′ has shifted to slightly lower wavenumbers (~1630 cm^{-1}), while the amide II′ band, giving rise to the so called residual amide II, and appears significantly decreased in intensity. (77-78)
Calculation of the second derivates of both spectra show that the amide I and amide I′ consist of partly overlapping bands originating from the different secondary elements in the protein structure. (79-80) The intense and sharp band at 1630 cm^{-1}, together with the weak but equally sharp signal at 1690 cm^{-1} can be assigned to anti-parallel β-sheets. (81, 82) When compared to the corresponding bands in the spectrum recorded in normal water, these bands, (83) appear slightly shifted to lower wavenumbers. This is a common phenomenon observed in proteins prepared in deuterated buffers, and can be ascribed to exchange of amide protons for deuterons in solvent-accessible secondary structures and unordered segments, as described in above. This is confirmed by the significant decrease in the residual amide II intensity at ~1550 cm^{-1}, suggesting that extensive $^{1}H/^{2}H$ exchange has occurred during preparation of the sample at 4°C. The less intense and less resolved bands at 1671 and 1680 cm^{-1} may be associated to turns and/or β-sheets. (84,29,38) The remaining signals below 1620 cm^{-1} can be assigned to specific side chain absorptions, such as 1605 (Tyr, as phenolate), (85) 1565 (ionised Glu) (85) and 1515 cm^{-1} (Tyr).(85) The resolution-enhanced spectra of bAGP are similar to the ones previously obtained from hAGP studies by FT-IR.(86) To estimate the secondary structure content of the protein, a curve-fitting procedure on the deconvoluted spectrum of bAGP analysed in $^{2}H_2O$ at 20°C (Fig. 3.1C) was performed. The secondary structure composition was found to be 35-40 % β-sheets, 21 % α-helices, 29 % unordered structures and 10-15 % β-turn (Figure 3.1 C).

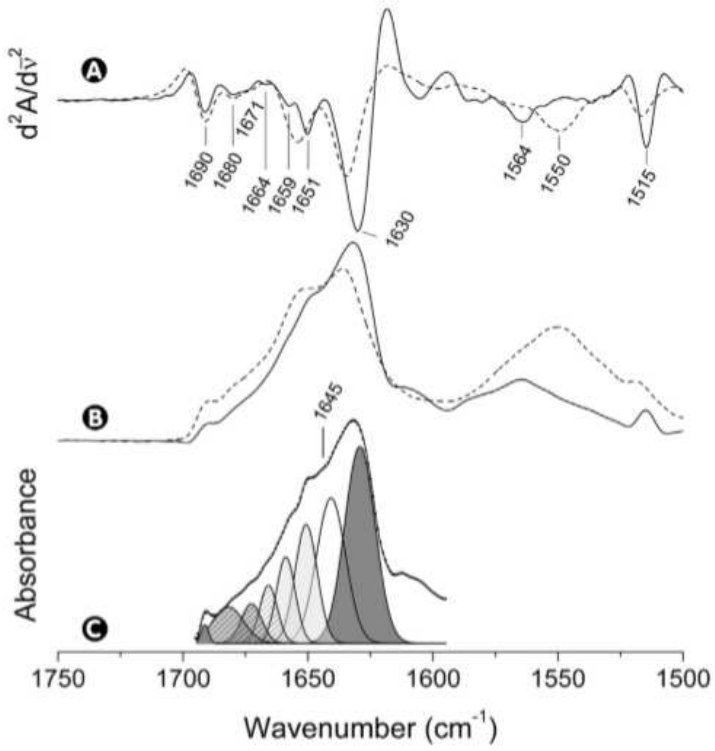

Figure 3.1. Second derivative (A), self-deconvoluted (B) and curve-fitting spectra of b-AGP (C). Spectra were recorded at 20 °C, in H_2O (dashed lines) and ^2H_2O (continuous lines) medium at pH and p^{2}H 7.4, respectively. Component bands assigned to β-sheet, α- helices and random coils (C) are shaded dark grey, light grey and white, respectively. Bands due to β-strands and/or turns are shaded in grey and striped. The dotted line represents the sum of the individual component bands. (29)

3.2 THERMAL UNFOLDING PATHWAY OF BOVINE AGP AT NEUTRAL p^{2}H

Infrared absorption spectra are able to show details on the process of protein denaturation, provided that the appropriate spectral regions are investigated. The amide I′ (1700-1600 cm^{-1}) and residual amide II′ (~1550 cm^{-1}) bands of samples prepared in deuterated media are reported bands to detect changes in secondary structure and overall flexibility/compactness induced by destabilizing conditions, such as temperature increases, as described in Paper I for human and bovine AGP. Other bands may be used, e.g. the Amide III (87) or the tyrosine vibration near 1515 cm^{-1} (88) but their interpretation is less straightforward. Protein denaturation often involves concerted and cooperative loss of its secondary structure elements. If studied by means of infrared spectroscopy, this alters the line shape of the amide I′ mode, due to the disappearance of the component bands ascribable to the different types of secondary structure.

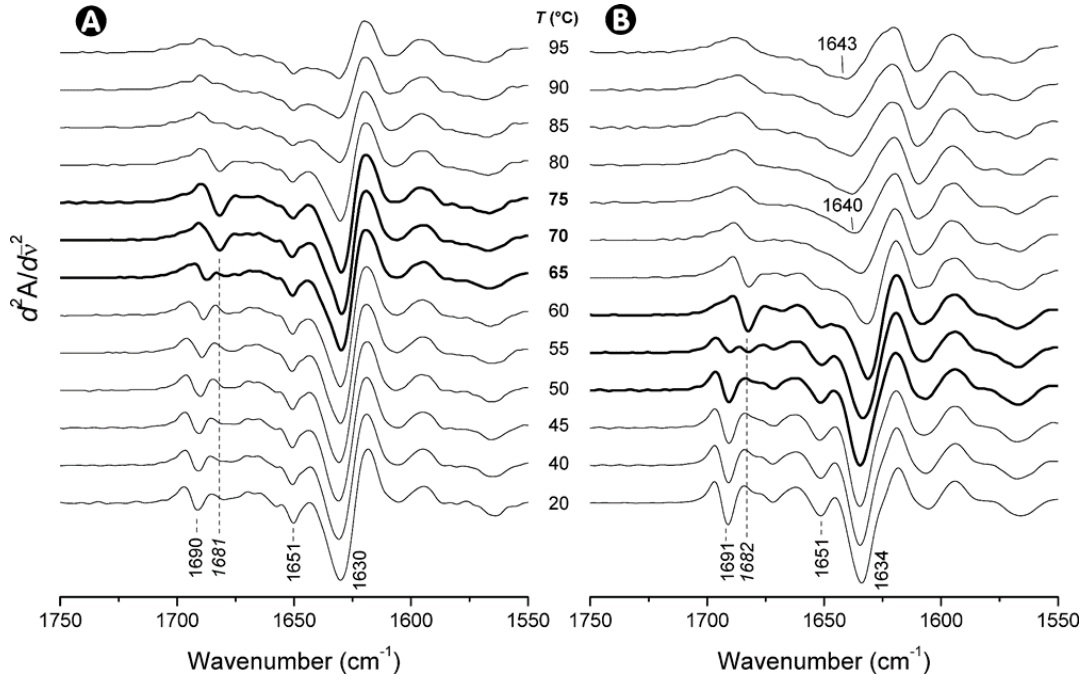

Figure 3.2. Second derivative spectra of b-AGP (A) and h-AGP (B) from 20 to 95 °C at p^{2}H 7.4.

Information on the thermal stability of proteins can be obtained by monitoring the second derivatives as a function of temperature. The second derivative spectra of bAGP (Figure 3.2A) show that the protein maintains its secondary structure up to 75 °C, as no significant decrease in band intensities in the amide I′ region can be observed. For instance, the intensity of the main β-sheet band (1630 cm^{-1}) remains unchanged up to 75 °C, and it starts to decrease significantly only at 80°C. At 80°C, the main β-sheet band starts to decrease in intensity, indicating that at this temperature the protein starts to denature. Denaturation proceeds above 80 °C, and can be observed in the form of a continuous decrease in intensity of the bands in the amide I′ region, indicating loss of secondary structure. It is noteworthy that at the highest temperature investigated (95 °C), bAGP is not completely denatured (Fig. 3.2A), as indicated by the presence of weak bands at 1651 and 1630 cm^{-1}, ascribable to α-helix and β-sheet structures, respectively. The spectra of hAGP (Fig. 3.2B) show that the intensity of the main β-sheet band (1634 cm^{-1}) remains almost the same up to 60°C, and it starts to decrease significantly only starting from 65 °C. At 65°C, the decrease in intensity of the bands due to α-helix and β-sheet structures is evident, while from 70 °C and above loss of secondary structure is complete and a band around 1640 cm^{-1} defines the spectrum of human AGP. At 95 °C this band becomes broad and centered at 1643 cm^{-1}, a frequency that is characteristic of unordered structures. (89,80,82) In view of these observations, it is clear that bAGP and hAGP have a very similar pathway of thermal unfolding at neutral p^{2}H, but the bovine protein is significantly more thermostable than its human counterpart.

3.3 EFFECT OF p^{2}H ON THERMAL STABILITY OF BOVINE AND HUMAN AGP: INFLUENCE OF DISULFIDE BRIDGES

More detailed information can be obtained by calculating difference spectra from the absorption spectra recorded at increasing temperatures. A difference spectrum is obtained by subtracting the absorption spectrum recorded at a certain temperature, T_i, from the spectrum recorded at the next temperature value, T_f. The resulting spectrum, T_{f-i}, allows to detect even the minutest structural changes occurring in that temperature interval. Indeed, positive bands represent bands the intensity of which increases as the temperature increases, while negative bands correspond to disappearing bands. Particular patterns of negative and positive bands may indicate band shift. One of the advantages of resorting to difference spectra is that all bands are silenced but those whose spectral features (intensity, position and/or width) are altered by the applied perturbation. This is of outstanding utility when hand ling intrinsically crowded spectra, such as those displayed by proteins.

The structure and thermal stability of bovine AGP was investigated at four p^{2}H values different to neutrality: 4.5, 5.5, 7.4 and 10. (Figure 3.3)(29)

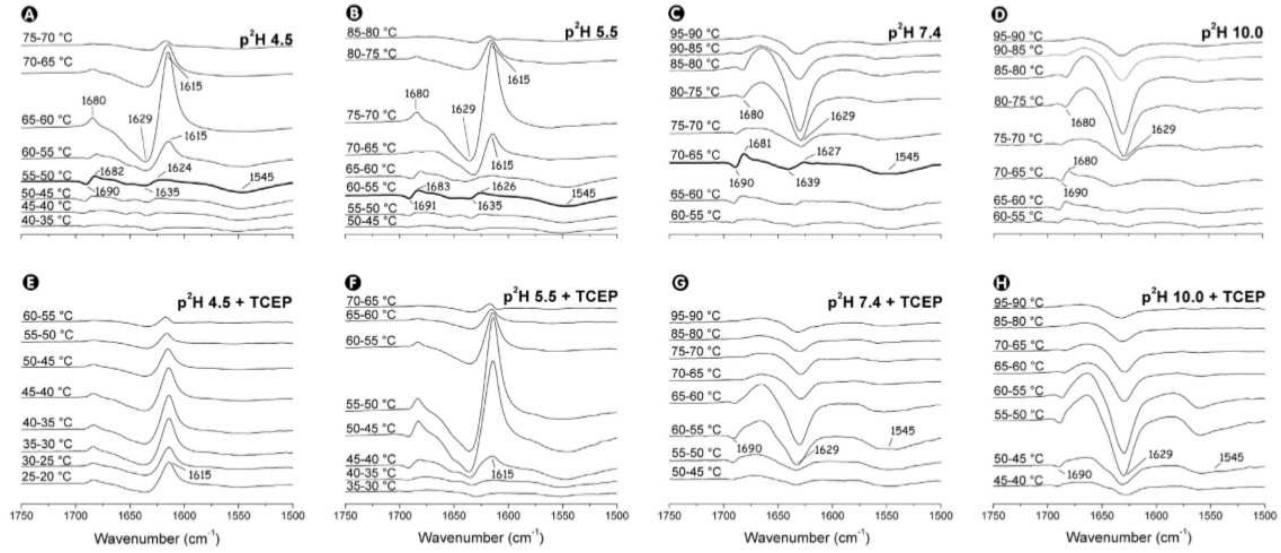

Figure 3.3. Difference spectra of bAGP at different p^{2}Hs in the absence (A-D panels) and in the presence (E-H panels) of the reducing agent TCEP. Bold lines highlight the difference spectra that describe the presence of the Molten Globule state.

In difference spectra, negative bands in the amide I′ region are associated with protein denaturation, while two positive bands close to 1615 (strong) and 1680 (small) cm^{-1} originate from protein aggregation. In some case, the presence of adjacent positive and negative bands of similar intensity is associated with band shifting (90, 46) This is due to further ^{1}H/^{2}H exchange of backbone amides that occurs as a consequence of relaxation of protein structure. Indeed, proteins dissolved in heavy water at room temperature do not exchange completely amide hydrogens with deuterium. If relaxation of protein structure occurs, the buried backbone amides become accessible to the solvent (^2H_2O) and further ^{1}H/^{2}H exchange takes place. This is revealed by a negative broad band close to 1550 cm^{-1}. (90) At p^{2}H 4.5 (panel A) and p^{2}H 5.5 (panel B), a band shifting to lower wavenumbers of the high and low frequency bands of anti-parallel β-sheets can be observed (bold lines at 55-50

°C and 60-55 °C, respectively), together with a broad, negative signal around 1545 cm^{-1}, indicating enhanced $^{1}H/^{2}H$ exchange of backbone amides due protein structure relaxation. This behavior, together with the absence of evident secondary structural changes ascribable to protein denaturation, may indicate the presence of a temperature-induced molten globule-like state (MG), typically characterised by unchanged secondary structure and a relaxed tertiary structure. (91) A similar small IR signal (70-65 °C) can be seen at $p^{2}H$ 7.4, whilst at $p^{2}H$ 10.0 only the shifting of the high frequency anti-parallel β-sheet band (1690/1680 cm^{-1} bands) can be clearly observed. Even smaller signals are present at temperatures below those indicated by the bold lines, suggesting that the relaxation of protein structure occurs in a broad range of temperatures. A temperature-induced molten globule-like state has been detected previously in thioredoxin (92) and in different lipocalins such as porcine odorant binding protein, (93) bovine and rat odorant binding protein (94) and hAGP. (29)

Strong IR signals related to band shifting were detected in all above cited cases. In the case of bovine AGP the IR signals are small and in some cases not very clear. This could be due to different and complex factors that may affect the difference spectra (49) such as band broadening/ narrowing and protein compactness. In particular, at room temperature a flexible, less compact protein undergoes $^{1}H/^{2}H$ exchange to a larger extent than a less flexible, more compact protein. Thus, at high temperature the band shift will be small because a few residual amide hydrogens will be exchanged with deuterium and, as a consequence, the IR different spectra will show small signals. The 1629 cm^{-1} negative broad band present in left panels, indicate protein denaturation. The onset of denaturation is shown by the (60-55), (70-65), (75-70), (75-70) difference spectra at $p^{2}H$ 4.5, 5.5, 7.4 and 10.0, respectively. At $p^{2}H$ 4.5 and $p^{2}H$ 5.5 protein denaturation is accompanied by protein aggregation, as revealed by the strong (1615 cm^{-1}) and small (1680 cm^{-1}) positive peaks. (95)

On the other hand, the unfolding of bovine AGP is not accompanied by protein aggregation at both $p^{2}H$ 7.4 and $p^{2}H$ 10.0. The temperatures at which bAGP exists in a relaxed conformation are lower at acidic $p^{2}Hs$ than at $p^{2}H$ 7.4, suggesting that the formation of MG state correlates with thermostability, and that probably they both depend on the protonation state of the protein.

Thermal unfolding studies were carried out also in the presence of the reducing agent TCEP at the $p^{2}H$ values described above (Figure 3.3, panels E-H). bAGP has five cysteines involved in two disulfide bridges (Cys5–Cys148 and Cys73–Cys166). It is noteworthy that Cys59 protrudes to the barrel towards the solvent. The model proposed in the Paper I (Figure 3.4) shows that the disulfide bridges anchor the protein termini to the protein scaffold. (29) More specifically, disulfide Cys5–Cys148 anchors the N-terminus to the long α-helix flanking the β-barrel, while disulfide Cys73–Cys166 anchors the C-terminus to strand D. Disulfide bridges have been shown to play a pivotal role in the stability of the lipocalin scaffold in human AGP (23), as well as in other proteins belonging to the same superfamily. More specifically, it has been postulated that the two disulfide bridges in human AGP are involved in tethering a long C- terminal loop to the lipocalin scaffold. (23)

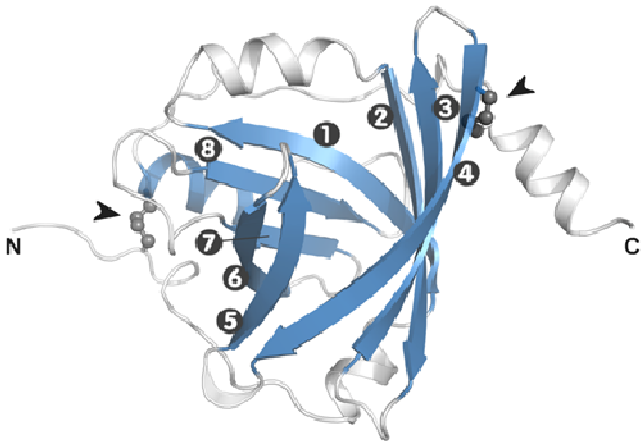

Figure 3.4. Proposed model structure of bovine AGP: 3D secondary structure elements making up the typical lipocalin fold. β-strands are labelled 1-8. Arrowheads denote the disulfide bridges. (29)

These disulfide bonds are conserved in the proposed model of bovine AGP, which leads to the hypothesis that they may, in a similar way, be involved in the structure and stability of the protein. Treatment with TCEP significantly decreases the thermal stability of bovine AGP at p^2H 7.4 and 10.0.For p^2H 7.4 + TCEP the two negative signals at 1629 cm^{-1} (strong) and 1690 cm^{-1} (weak), corresponding to denaturation of the native anti-parallel β-strands, are now observed starting from 55 to 50 °C (Figure 3.3, panel G) while at p^2H 10.0 + TCEP these signal patterns are observed starting from 50 to 45 °C (panel H). Reducing conditions are negative for the thermal stability also at acidic pHs. At p^2H 5.5 + TCEP the typical aggregation band at 1615 cm^{-1} is now observed in the difference spectrum starting from 45 to 40 °C (panel F) while at p^2H 4.5 + TCEP the aggregation band appears already in the difference spectrum at 25-20 °C (panel E). Remarkably, in the difference spectra in the presence of TCEP the spectral changes associated to the relaxation of protein structure are now not visible (panels E-G). This may suggest that disulfide bridges are essential for the thermal stability of bovine AGP and its ability to form intermediate states.

4. RESULT AND DISCUSSION: AMYLOID FIBRILS

The infrared measurements of temperature-induced denaturation of bAGP at different p^{2}H and disulfide oxidation states described in Paper II revealed that p^{2}H values below neutrality and reduction of the disulfide bridges lead to aggregation of the polypeptide chains with formation of anti-parallel, intermolecular β-sheets. The disulfide bridges have been shown to markable stabilizing effect, since treatment with reductant leads to a significant increase of the aggregation propensity. In this chapter, results showing the amyloid nature of aggregated AGP are presented, aimed at providing a molecular explanation for the observed assembly of monomeric AGP into fibrils. The data presented here have been adapted from Paper II.

4.1 AGGREGATION OF BOVINE AGP MONITORED BY INFRARED SPECTROSCOPY

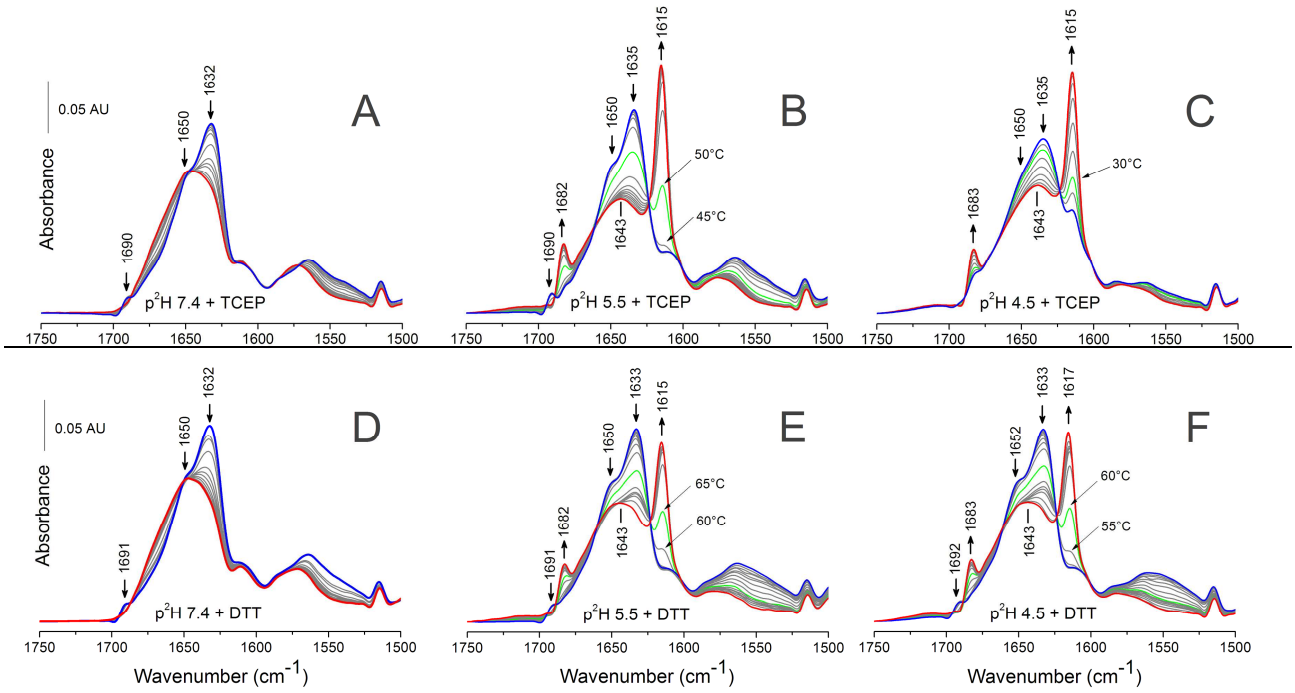

Figure 4.1. Deconvoluted infrared spectra of bAGP recorded during thermal denaturation at p^{2}H 7.4, 5.5 and 4.5 in the presence of 5 mM TCEP or DTT. (96)

Deconvoluted infrared spectra in Figure 4.1 were recorded every 5 °C intervals. Blue lines denote spectra recorded at 20 °C, while red lines denote spectra recorded at 95 °C (panels A-C and D-F) or 60 °C (panel C). The arrows ↑ and ↓ indicate the increase and decrease, respectively, of the corresponding band intensities. The nature of the bands composing the amide I′ has been discussed previously. Briefly, the signals close to 1635 and 1691 cm^{-1} can be assigned to the native, anti-parallel β-strands assembled in the barrel, while the signal at 1651 cm^{-1} can be assigned to α-helices. Both in the presence of TCEP or DTT, increases in temperature lead to the disappearance of the secondary structure bands described above, with the concomitant appearance of bands ascribable to anti-parallel, intermolecular β-sheets (1615 and 1683 cm^{-1}) and to random coils (1643

cm^{-1}), suggesting denaturation and aggregation. In the presence of DTT (panels D-F), the spectra of bAGP at p^2H 5.5 and 4.5 show the onset of aggregation at higher temperature (60 °C and 55 °C, respectively) respect to the spectra of the protein in the presence of TCEP (panels A-C)(45 °C and 20 °C, respectively). This result, most likely is due to the lower reducing efficiency of DTT (96) and consequently to its lower ability to destabilize the protein structure.

In synthesis, the data obtained by infrared spectroscopy indicate that under reducing conditions, bovine AGP is destabilised at increased medium acidity, and that at p^2H 4.5 significant destabilisation of the protein structure already occurs at 20 °C in the presence of reductant. The infrared data also show that below neutrality, denaturation is accompanied by aggregation of the polypeptide chain.

4.2 KINETICS OF FIBRIL FORMATION

Protein aggregation pathway can be assessed by monitoring the dependency of a structural parameter as a function of temperature. This approach is to consider the intensity of a particularly abundant type of secondary structure in resolution-enhanced spectra. Insights on the thermal stability of bAGP can thus be obtained by measuring the intensity of the native β-sheet band at 1630 cm^{-1} in the second derivative spectra. In a similar way, plotting the intensity of the aggregation band at 1616 cm^{-1} against temperature can provide information on the progress of aggregation during heating of the sample.

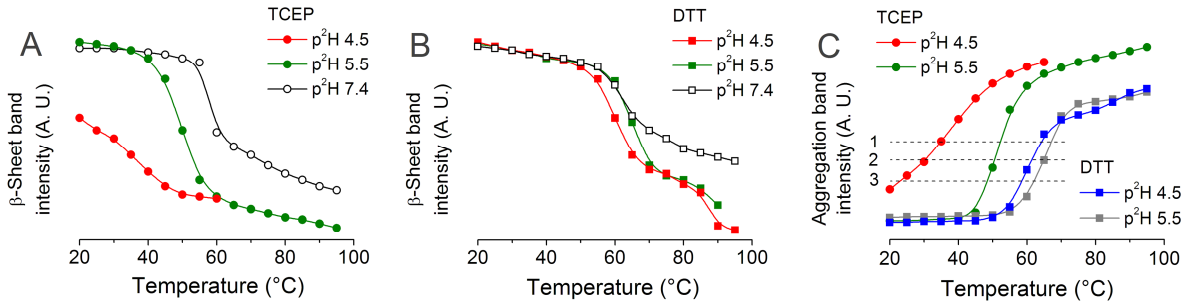

Figure 4.2. Thermal denaturation (A and B) and aggregation (C) curves of bovine AGP at different p^2Hs and in the presence of TCEP (A) or DTT (B).
Panel (C) shows the aggregation band (close to 1615 cm^{-1}) intensities as a function of temperature. The intersection of dashed line 1, 2 and 3 with the aggregation curves highlights the temperatures at which for each experiment the aggregation band intensity is the same. Line 1, from the left to the right: 32, 51, 64, 67 °C. Line 2, from the left to the right: 27, 49, 61.5, 65 °C. Line 3, from the left to the right: 21, 47, 58,6, 62 °C.

Aggregation is the most common phenomenon for proteins undergoing thermal unfolding. (97) Amorphous aggregates and amyloid fibrils cannot be discerned by only interpretation of their infrared spectra because they possess similar secondary structure, thereby giving rise to similar absorptions in the amide I′ region. To assess whether bAGP forms amorphous or amyloid-type aggregates we performed both TEM analyses and Thioflavin T (ThT) binding experiments (figure

4.3). The TEM micrographs (Figure 4.3, panel A, B) show that the reduced protein adopts different morphologies, such as large aggregates with a fine fibrillar structure or long fibrils. (96)

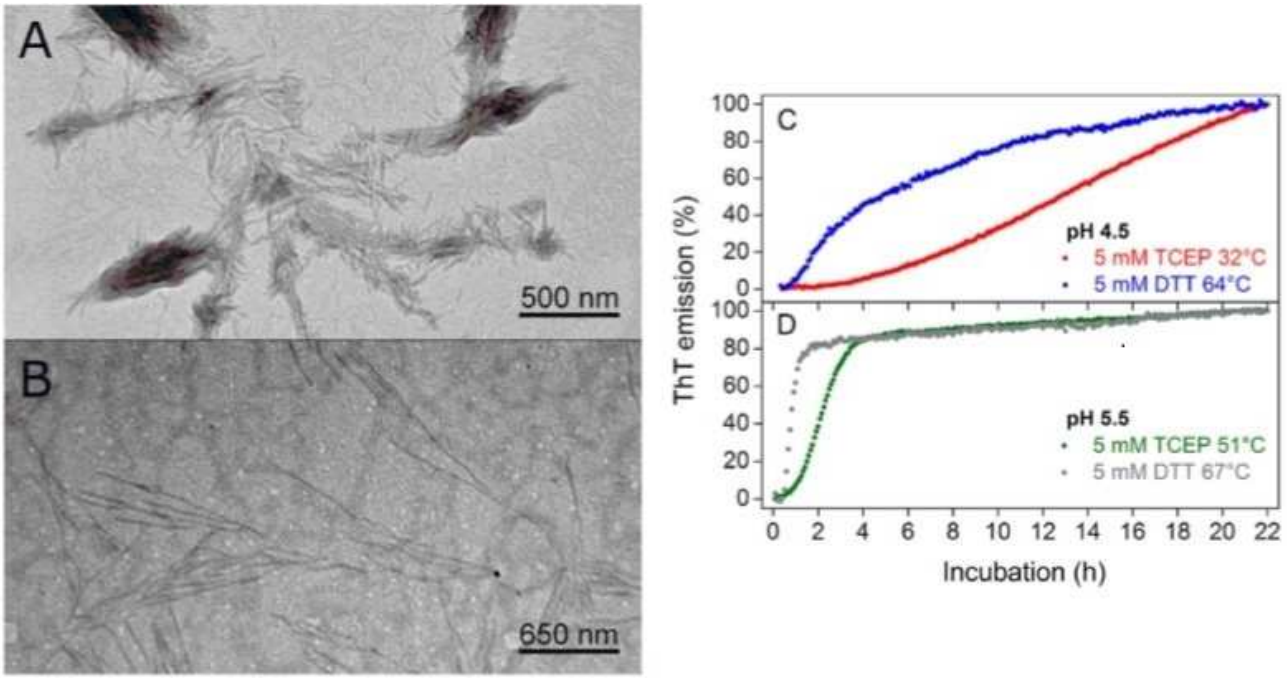

Figure 4.3. Fibril morphology as observed by TEM (A, B) and Time-dependent change in the fluorescence emission of ThT in the presence of 0.1 mg mL^{-1} non-pre-reduced-bAGP under different conditions (C, D). Panels A and B show TEM micrographs of the protein obtained under the same conditions as in C and D.

Thioflavin T (ThT) is a fluorescent probe often used in the characterization and detection of amyloid fibrils *in vitro* and *ex vivo*. (71) When free in solution, ThT is only weakly fluorescent. Upon binding to cross-β structures, the recurring structural motif of amyloid fibrils, (98-100) the fluorescence emission of the probe increases several fold, concomitantly red-shifting its emission maximum to 480- 490 nm. (101)

In time-dependent ThT-binding assays, the extent of fibril formation over time can be inferred from the intensity of the probe fluorescent emission. Fitting to appropriate functions allows to discriminate among the possible polymerization mechanisms, e.g. nucleation-dependent or independent, and to calculate kinetic parameters. The ThT experiments were carry out using DTT rather than TCEP to test the influence on fibril formation. The incubation temperatures were those corresponding to the similar aggregation as determined by FT-IR, (Figure 4.2C, line 1) in order to normalise for a comparable folded/unfolded state of the protein. In all samples, the fluorescence emission of ThT increases over time, indicating formation of amyloid fibrils. Figure 4.3 (panel C, D) shows the presence of a lag phase with a similar duration in all cases (0.4 – 0.9 h.), except the experiment at pH 4.5 in the presence of TCEP which shows a longer lag phase (3.8 h). This result might be explained as follows: in the latter case the experimental temperature was lower than the T_m whilst in the other cases was above T_m values (data not shown). As a consequence, the protein structure would be less destabilised and the disulphide bridges reduction less efficient.

4.3 LAG PHASE PRESENCE: SEEDING TRIALS

In fibrillation processes, the presence of a lag phase corresponds to formation of nuclei, which represent a thermodynamic block for the full process of fibril assembly, usually requiring stable, soluble monomers to overcome high energy barriers. (102) Downstream recruitment of monomers onto existing nuclei is, however, energetically favourable because it gives rise to more stable structures with extensive H-bonding networks, such as fibrils or protofibrils. The presence of a lag phase in the ThT-binding kinetics thus calls for a nucleation-dependent mechanism (102) to explain fibril formation by bAGP. To assess this hypothesis, seeding trials were performed by incubating the protein in the presence of freshly sonicated fibrils, as described elsewhere in the literature. (103)

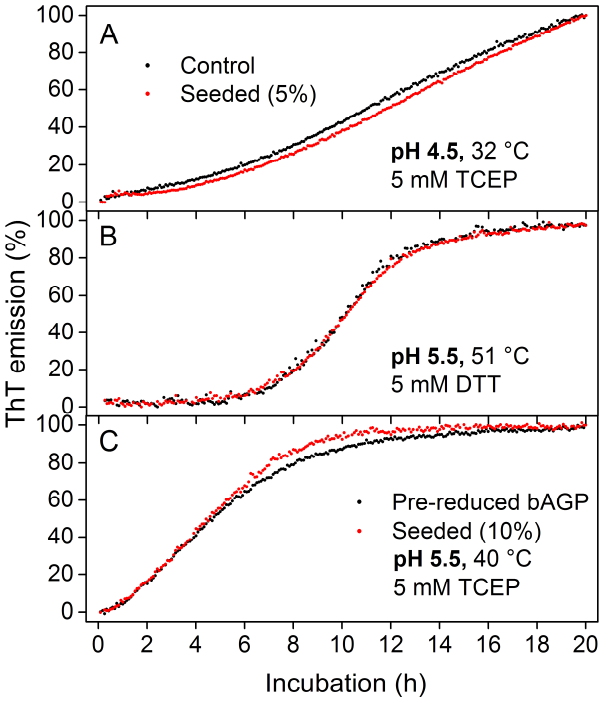

Figure 4.4. Effect of seeding on the kinetics of fibril formation by non-pre-reduced-bAGP (panel A, B) or pre-reduced-bAGP (panel C) under different conditions. The black curves are the control and the red curves are different percentage of seeded. The emission intensity at t=0 h was subtracted from all points, and the resulting emission intensity at t =20 h was considered as 100%.

In spite of their stability, mature fibrils can be broken down to fragments, or seeds, by extensive sonication. According to many authors, seeds can mimic nuclei by providing a structural template that rapidly reforms the fibril by recruiting soluble monomers. This often significantly reduces, and sometimes completely abolishes, the observed lag phase, as reported for several amyloidogenic proteins, such as β_2-microglobulin (104), the Aβ peptide (105) and lysozyme (106), only to name a few examples.

In these experiments, seeding neither abolished nor reduced the lag phase observed during fibrillation of not reduced bAGP at pH 4.5 or pH 5.5 (Figure 4, A and B), despite a seed

concentration higher than those commonly used by other authors (0.1–2%). In both cases, the plots obtained with the seeded sample are nearly or completely superimposable to the respective controls, indicating that the aggregation process does not fit with a Nucleation-Dependent Polymerization (NDP) model.

4.4 ROLE OF DISULFIDE REDUCTION

Addition of seeds failed at shortening the lag phase observed at both pH 4.5 and 5.5, suggesting that the lag phase is due to a phenomenon different to formation of nuclei or other types of oligomers. On the other hand, it is noteworthy that the duration of the lag phase seems to be dependent on the accessibility of the reducing agent to the disulphide bridges, i.e. on the destabilization degree of the protein (Figure 4.5). To further validate this hypothesis, the fibrillation assay was repeated using fully reduced bAGP obtained by prior incubation of the protein with TCEP or DTT under non-aggregating conditions (Figure 1 panels A, D; pH 7.4, 65 °C). Under these conditions, bAGP undergoes unfolding (Figure 1, panel A, T_m = 59.6 °C and panel D, T_m = 63.8) and the reductant can easily reduce the disulphide bridges. The reduced and unfolded protein at pH 7.4 is, however, not likely to aggregate as indicate by the IR data, which do not show the aggregation signals (Figure 1 panels A and D). The use of pre-reduced bAGP (PR-bAGP) in fibrillation experiments completely abolished the lag phase, and produced a trend that is best fitted with a first order exponential decay function, rather than with a sigmoidal function (figure 5).

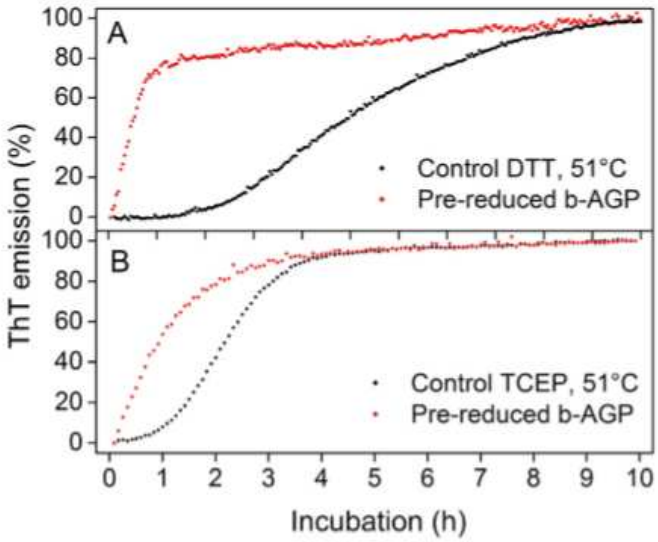

Figure 4.5. Effect of pre-reduction on the kinetics of fibril formation by bAGP at pH 5.5, 51 °C in the presence of DTT (A) or TCEP (B). The emission intensity at t = 0 h was subtracted from all points, and the resulting emission intensity at t = 10 h was considered as 100%. Control bAGP in presence of DTT and TCEP (black points); fibrillation kinetics of pre-reduced bAGP (red points).

Consistently with the worthless effect of seeding, this type of fibrillation kinetics can be ascribed to a nucleation-independent mechanism. A possible, alternative mechanism might involve conversion of a stable, soluble monomer into an aggregation-prone conformer which is able to trigger the fibrillation process. This occurs, for instance, in downhill polymerization mechanisms, as reported for some amyloidogenic proteins such as transthyretin (107), bovine (108) and human serum albumin (109), among others. This mechanism involves transformation of the native protein into an amyloidogenic monomer that assembles into soluble aggregates which lead to fibrillation. In our case, the amyloidogenic monomer is represented by the reduced form of bovine AGP.

4.5 KINETIC ANALYSIS OF BOVINE AGP FIBRILLATION

The ThT binding assays and the seeding trials described above suggest a nucleation-independent polymerization mechanism for fibrillation of bAGP. Comparison of the fibrillation time-courses of "native" (non-pre-reduced) and pre-reduced bovine AGP might indicate that reduction of the disulfide bridges, if occurring under amyloid forming conditions, can change the kinetics of fibril formation and obstruct the analysis of the underlying molecular mechanism. The following analysis proposes a demonstration allowing for correct interpretation and modelling of the experimental data in complex fibrillation kinetics, such as those of bovine AGP as well as other amyloidogenic proteins containing disulfide bridges.

Nucleation-independent polymerization mechanisms, such as those attributed to human (23) and bovine AGP, lead to first-order exponential decay kinetics. This type of kinetics is compatible with a mechanism in which aggregation-prone AGP molecules are recruited by and attach to growing fibril ends. The rate at which fibrillation proceeds is proportional to the rate of disappearance of the free monomer, reversed in sign, and they both depend on monomer concentration.

The differences in thermal stabilities shown by bovine AGP in the reduced and unreduced states makes it possible to adjust the experimental conditions so as to trigger aggregation starting from either disulfide redox state (i.e. containing reduced cysteines, -SH, or disulfide bridges, S-S). For instance, at pH 4.5 or 5.5 and at T ~50 °C, the reduced form of the protein is the only one able to aggregate. The process of fibril formation by reduced bovine AGP can, therefore, be thought to occur according to the following system:

Unreduced state → Aggregation prone monomers → Fibrillation reaction

If reduction occurs concomitantly with the fibrillation reaction, then the process of fibril formation from unreduced AGP becomes a series of two subsequent reactions, as shown in the previous scheme. Chemical reduction of bovine AGP by treatment with TCEP or DTT follows first-order exponential decay kinetics provided that two assumptions are made: (1) the concentration of the reducing agent does not change over time because, for instance, it is present in large excess with respect to the protein; (2) reduction of either disulfide bridge is sufficient to trigger aggregation. (96)

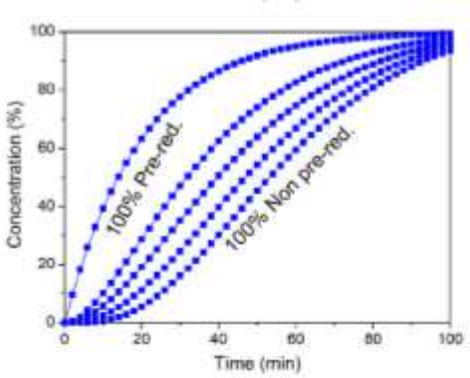

Figure 4.6. Calculated kinetics of bovine AGP fibrillation at different ratio of pre-reduced and not pre-reduced protein ratios: 100/0, 75/25, 50/50, 25/75, 0/100 pre-reduced/ non pre-reduced bAGP.

Figure 4.6, shows the calculated time-dependent changes in the fibrillation process when $k_{agg} > k_i$, assuming that the protein is present entirely in the unreduced state at t = 0 (where k_{agg} is the rate constant associated with the aggregation process and k_i is the rate constant associated with formation of the cysteine-reduced, aggregation-prone kinetic intermediate). It can be observed that reduced species accumulates during the early phase of the process, thereby decaying to 0 as the rate of reduction approaches 0 (at $t \rightarrow \infty$) and the reduced protein is consumed to form fibrils. The time-dependent change in the aggregated state of the protein shows a pseudo-sigmoidal trend and an apparent lag phase.

Assuming that the initial sample contains a mixture of reduced and non-reduced protein at t = 0, the rate of fibril formation depends on the rate of consumption of the monomers already reduced, as well as on the rate of formation/consumption of the newly reduced monomers obtained in situ by treatment with the reducing agent. In this case, the time-dependent value of the concentrations of the reduced state and fibrillation reaction is given by the ratio of concentration of the reduced species/monomeric state at t = 0: low ratios give pseudo-sigmoidal curves with longer apparent lag phases (arrowheads), while high ratios give first-order exponential decay curves with no or short lag phases (Figure 4.7, panels A-E). (96)

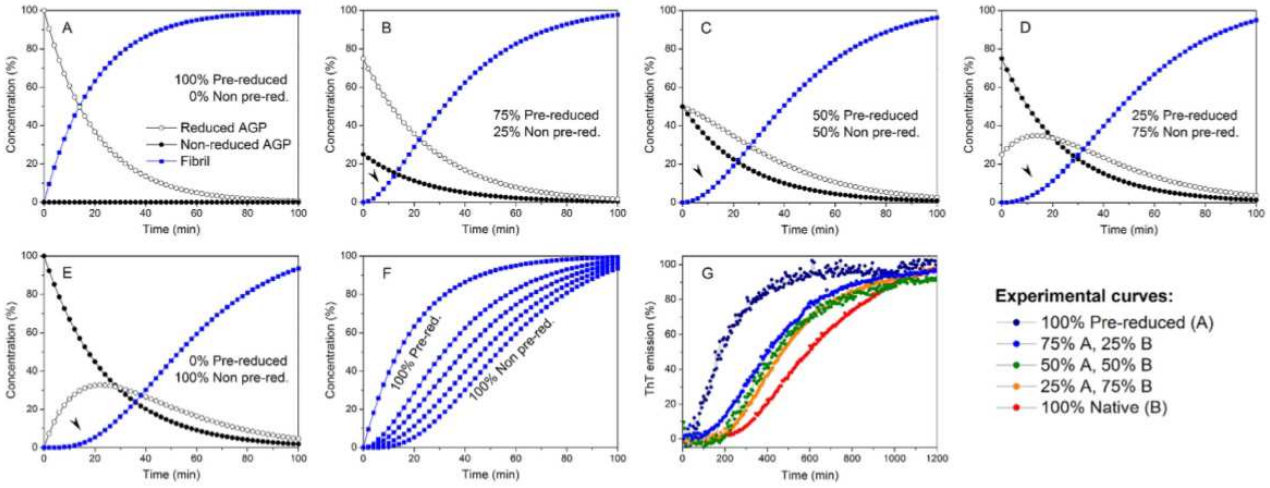

Figure 4.3. Calculated and observed kinetics of bovine AGP fibrillation at different concentrations of pre-reduced and not pre-reduced protein. Panels A-F: calculated kinetics at different initial ratios. Panel G: experimental ThT-binding kinetics obtained at the same ratios shown in panels A-F. Arrowheads indicate a lag phase.

Figure 4.7, panels A-E, shows the theoretical results obtained with the reduced species /monomeric state ratios:

(A) 100/0,

(B) 75/25,

(C) 50/50,

(D) 25/75,

(E) 0/100.

The time-dependent changes in the protein in the aggregated state for each of the previous cases are summarised in panel F. The calculated kinetics in panels A and E yield very similar plots to experimental ThT-binding measurements performed under reducing conditions at the same ratios of pre-reduced and unreduced bovine AGP (panel G), in which the apparent lag phase observed at low ratios of pre-reduced protein disappears to give trends showing a more pronounced single-exponential decay feature as the ratio of the pre-reduced protein increases. The result of this analysis is two-fold. On the one hand it confirms our previous observations that the initial redox state of the disulfide bridges in bovine AGP can have a dramatic effect on the kinetics of fibril formation. An incorrect interpretation of the kinetic data may lead to an erroneous aggregation mechanism. On the other hand, these results also show that it is possible to model aggregation kinetics of binary mixtures containing two forms (reduced and native) of the same amyloidogenic protein.

5. CONCLUSIONS

The research performed during my doctoral studies has been directed towards a better understanding of the structure and functions of bovine α_1-acid glycoprotein (bAGP) or orosomucoid, an important lipocalin involved in the acute phase response. Fourier Transform infrared (FT-IR) spectroscopy has been the experimental tool of choice, for several reasons. Probably, the most useful advantages of FT-IR spectroscopy exist in the possibility to simultaneously probe the secondary and tertiary structures of proteins prepared in heavy water, the low demand in terms of sample amount, and its intrinsic sensitivity towards β-structures. The latter feature makes it of unmatched utility in the study of β-rich proteins, such as lipocalins. The results obtained from the investigation of bAGP mostly regards two aspects of this protein, i.e. the occurrence of molten globule intermediates in the temperature-induced denaturation pathway and the ability to aggregate into fibrillar structures. The presence of a molten globule like-state in the thermal unfolding pathway of human AGP has been extensively described in previous works by our group. This intermediate state can be described in bAGP at p^2H values from 4.5 to 7.4 under non- reducing conditions. The temperature intervals in which bAGP assumes a molten globule-like conformation is strictly correlated to its p^2H-dependent thermostability and to the presence of disulfide bridges. Indeed, thermal unfolding experiments at p^2H values in the range 4.5 to 10.0 were performed in the presence of a reducing agent. The strong decrease in thermostability measured under these conditions suggests that not only do the disulfide bridges exist in the native structure, but that they also play a crucial role in stability and, most importantly, are essential for the formation of folding intermediates by bovine, as well as human AGP. Results stemming from this line of research make up the core of Paper I.

Aggregation is another important p^2H-dependent feature observed during denaturation. In particular, p^2H values below neutrality induce aggregation of the protein following denaturation. However, no aggregation is observed at neutral or basic p^2H values, where denaturation was also found to be reversible. Elucidation of relationship between environmental conditions and stability of AGP is essential in those fields where practical and/or biotechnological uses of this protein can be envisioned. For instance, applications of AGP in chromatographic media for the clean-up of adrenergic drugs in biological samples have been described.

An additional line of research has focused on the aggregation of AGP into amyloid fibrils. Although countless fibrillogenic proteins are constantly being discovered, the ability of bovine AGP to form fibrils is of particular biological significance in the light of its high levels that make it the second most abundant protein in our blood after serum albumin. One of the most important findings described in Paper II is that some conditions, e.g. acidic p^2H and reduction of disulfide bridges, induce aggregation of bAGP into anti-parallel β-sheets. Although this type of secondary structure is present in both amorphous and amyloid fibrils, the “crystalline” organization of the latter allows binding of specific dyes, such as Thioflavin T. The amyloid nature of the bAGP aggregates is confirmed by both TEM images and Thioflavin T binding experiments. The kinetics of fibril formation, monitored by the extent of ThT binding over time, suggest that conversion of the native monomer into an aggregation-prone species self-assembles to form the fibril. In the case of bAGP, this species corresponds to the fully reduced form of the protein. Further support to the downhill polymerization (NP) mechanism was provided by the seeding experiments performed both on the non-pre-reduced and pre-reduced protein. Because the lag phase observed during seeding trails was

neither abolished nor decreased, a nucleation-dependent polymerization (NDP) mechanism was excluded.

A molecular interpretation of the role of disulfide bridges on the fibrillation kinetics of bAGP is that S-S reduction may facilitate formation of kinetic intermediates with low or no ThT binding properties. In particular, the two disulfide bonds in bAGP might restrict the flexibility of aggregation-prone regions which, following reduction, become more exposed and induce aggregation of monomers into fibrils.

A theoretical time-courses analysis of bAGP fibril formation was proposed allowing interpreting and modeling the experimental data at different ratios of pre-reduced and non-pre-reduced protein. The data are in agreement with experimental mixtures and show that the presence of an apparent lag phase, as well as its duration, depend on the presence of unreduced (i.e. native) protein with intact disulfide bridges at the beginning of the incubation under reducing conditions. The equations proposed in Paper II, therefore, allow for a more accurate kinetic analysis of fibril formation by bAGP, and can equally well be applied to interpret the kinetics of fibril formation by other amyloidogenic proteins containing disulfide bridges.

BIBLIOGRAPHY

1. D.R. Flower. J. Mol. Recognit. 8, 185–195 (1995)

2. D.R. Flower. Biochem. J., 318, 1–14 (1996)

3. S. Pervaiz, K. Brew. Science 228, 335-337 (1985)

4. S. Pervaiz, K. Brew. FASEB J. 1, 209-214 (1987)

5. B. Åkerstrom, D.R. Flower, J.P. Salier. Biochim Biophys Acta. 1482(1-2), 1-8 (2000)

6. P. Venge Scand. J. Clin Lab. Invest., 219, 47–54 (1994)

7. G. H. Fey and G. M. Fuller. Mol. Biol. Med. 4(6), 323–38 (1987)

8. L. Dente, M.G. Pizza, A. Metspalu, and R. Cortese. EMBO J. 6(8), 2289–96 (1987)

9. T. Kido, R. Honda, Y. Yamada, I. Tsuritani, M. Ishizaki, K. Nogawa Toxicol. Lett, 24, 195–201 (1985)

10. J. Pevsner, R.R. Reed, P.G. Feinstein, S.H. Snyder. Science 241(4863), 336-339 (1988)

11. P.A. Routledge. Prog. Clin. Biol. Res., 300, 185–198 (1989)

12. G.T. Waites, S.C. Bell J. Reprod. Fertil. 87, 291–300 (1989)

13. B. Åkerström Lipocalins Molecular Biology Intelligence Unit Landes Bioscience, (2006)

14. B. Lakshmi, M. Mishra, N. Srinivasan, G. Archunan. PLoS ONE 10(8), 0135507 (2015)

15. M. D. Ganfornina, G. Gutiérrez, M. Bastiani and D. Sánchez. Mol Biol Evol 17 (1), 114-126 (2000)

16. D.R. Flower. Benzon, 2, 235–236 (2003)

17. R.E. Bishop, S.S. Penfold, L.S. Frost, J.V. Höltje, J.H. Weiner J Biol Chem. 270(39), 23097-103 (1995)

18. D. Sánchez, M.D. Ganfornina, G. Gutiérrez, A. Marín. Molecular Biology and Evolution 20(5), 775-83 (2003)

19. D.R. Flower, A.C. North, C.E. Sansom. Biochim. Biophys. Acta 1482, 9-24 (2000)

20. D.R. Flower. Biochim. Biophys. Acta, 1482, 46–56 (2000)

21. A. Scirè, M. Baldassarre, G. Lupidi, F. Tanfani. Biochimie 93, 1529-1536 (2011)

22. K. Nishi, Y. Komine, N. Fukunaga, T. Maruyama, A. Suenaga, M. Otagiri. Proteins 63, 611-620 (2006)

23. A. Scirè, M. Baldassarre, R. Galeazzi, F. Tanfani. Biochimie 95, 158-166 (2013)

24. L. Logdberg, L. Wester. Biochim. Biophys. Acta 1482, 284–297 (2000)

25. K. Tamura, T. Yatsu, H. Itoh, Y. Motoi, N. J. Zasshi 51, 987-994 (1989)

26. M. Nakano, K. Kakehi, M. Tsai, Y.C. Lee. Glycobiology 14, 431–441 (2004)

27. D. R Flower. FEBS Lett 354(1), 7–11 (1994)

28. B. Akerstrom and L. Logdberg Trends. Biochem Sci 15(6), 240–3 (1990)

29. M. Baldassarre, R. Galeazzi, B. Maggiore, F. Tanfani, A. Scirè. Biochimie 102, 19–28 (2014)

30. F. Ceciliani, V. Pocacqua, C. Lecchi, R. Fortin, R. Rebucci, G. Avallone, V. Bronzo, F. Cheli, P. Sartorelli. J. Dairy Res. 74, 374-380 (2007)

31. F. Ceciliani, V. Pocacqua, E. Provasi, C. Comunian, A. Bertolini, V. Bronzo, P. Moroni, P. Sartorelli, 36, 735-746 (2005)

32. C. Lecchi, G. Avallone, M. Giurovich, P. Roccabianca, F. Ceciliani. Vet. J. 180, 256-258 (2009)

33. C.L. Fernandes, R. Ligabue-Braun, H. Verli. Glycobiology 25(10):1125-33 (2015)

34. S.I. Snovida, V.C. Chen, O. Krokhin, H. Perreault. Anal. Chem. 78, 6556-6563 (2006)

35. D.A. Breustedt, D.L. Schönfeld, A. Skerra. Biochim Biophys Acta. 1764(2), 161-73 (2006)

36. S. C. Paterson, C. K. Lim and K. D Smith. Biomed Chromatogr 17(2-3), 143–8 (2003)

37. F. Albani, R. Riva, M. Contin and A. Baruzzi. Br J Clin Pharmacol 18(2), 244–6 (1984)

38. E. Hazai, J. Visy, I. Fitos, Z. Bikadi and M. Simonyi. Bioorg Med Chem 14(6), 1959–65 (2006)

39. F. Hervè, J. C. Duche, P. d'Athis, C. Marche, J. Barre and J. P. Tillement. Pharmacogenetics 6(5), 403–15 (1996)

40. McNamara, P. J., Brouwer, K. R., and Gillespie, M. N. Biochem Pharmacol 35(4), 621–4 (1986)

41. D. Morin, N. Simon, P. Depres-Brummer, F. Levi, J. P. Tillement and S. Urien. Pharmacology 54(5), 271–5 (1997)

42. W. Chachaj, Z. Bartecka and J. Malolepszy. Arch. Immunol. Ther. Exp (Warsz) 28(6), 947–51 (1980)

43. S. Urien, E. Albengres, R. Zini and J. P. Tillement. Biochem Pharmacol 31(22), 3687–9 (1982)

44. J. L. Pinquier, S. Urien, P. Chaumet-Riffaud and J. P. Tillement. Br J Clin Pharmacol 28(5), 587–92 (1989)

45. K. V. Ponganis and D. R. Stanski. J Pharm Sci 74(1), 57–60 (1985)

46. J. P. Williams, M. R., Weiser, T. T. Pechet, L. Kobzik, F. D. J. Moore and H. B. Hechtman, Am J Physiol 273(1), 1031–5 (1997)

47. M.P. Vasson, M. Roch-Arveiller, R. Couderc, J.C. Baguet, and D. Raichvarg, Clin Chim Acta 224(1), 65–71 (1994)

48. M. Costello, B. A. Fiedel and H. Gewurz. Nature 281(5733), 677–8 (1979)

49. J. Valles, M. T. Santos, A. J. Marcus, L. B. Safier, M. J. Broekman, N. Islam, , H. L. Ullman and J. Aznar. J Clin Invest 92(3), 1357–65 (1993)

50. K. M. Chiu, R. F. Mortensen, A. P. Osmand and H. Gewurz, Immunology 32(6), 997–1005 (1977)

51. J. Wu, Y. X. Zeng and K. Hirokawa, Cell Signal 11(6), 391–8 (1999)

52. S.D. Shiyan, A.L. Pukhal'skii, A.P. Toptygina, V.V. Nasonov and N. V. Bovin. Bioorg Khim 20(8-9), 994–1000 (1994)

53. L. A. Lasky. Science 258(5084), 964–9 (1992)

54. Friedman, M. J. Proc Natl Acad Sci U S A 80(17), 5421–4 (1983)

55. A. Athamna, M. R. Kramer and I. Kahane. FEMS Immunol Med Microbiol 15(2-3), 135–41 (1996)

56. P.I. Haris, A. Barth, editors. Biological and Biomedical Infrared Spectroscopy. Amsterdam: IOS Press; pp 1–52 (2009)

57. Colthup, NB, Daly, LH, and Wiberley, SE, Introduction to Infrared and Raman Spectroscopy (San Diego, CA: Academic Press) (1990)

58. Umesh P.; Rajai H. Vibrational Spectroscopy Chapter 4. In Lignan and lignans: advances in chemistry; Heitner, Cyril; Dimmel, Donald R.; Schmidt, John A. eds; Taylor & Francis Group: Boca Raton; pp 103-136 (2010)

59. Stuart, B. Biological Applictions of Infrared Spectroscopy. Wiley, Greenwhich, (1997)

60. A. Barth, C. Q. Zscherp Rev. Biophys. 35, 369–430 (2002)

61. Heino Susi, D.Michael Byler Arch. Biochem. Biophys. 258, 465-469 (1987)

62. P. Chitnumsub, W.R. Fiori, H.A. Lashuel, H. Diaz, J.W. Kelly. Bioorg Med Chem.; 7, 39-59 (1999)

63. R. Rey, K. B. Moller, and J. T. Hynes, J. Phys. Chem. A, 106, 11993–11996 (2002)

64. C.J. Fecko, J.D. Eaves, J.J. Loparo, A. Tokmakoff, P.L. Geissler Science. 301, 1698-1702 (2003)

65. P. L. Silvestrelli, M. Bernasconi, M. Parrinello. Chem. Phys. Lett., 277(5–6), 478–482 (1997)

66. Heinz Fabian and Werner Mäntele Infrared Spectroscopy of Proteins. In handbook of vibrational spectroscopy Chalmers, J. M. and Griffiths, P. R. (Eds), Wiley, Chichester, UK, 3399-3426 (2002)

67. Safford, William Edwin (1916). "Lignum nephriticum". Annual report of the Board of Regents of the Smithsonian Institution (PDF). Washington: Government Printing Office. pp. 271–298

68. Lakowicz, Joseph R. (1999). Principles of Fluorescence Spectroscopy. Kluwer Academic/Plenum Publishers pp. 10

69. Valeur, Bernard, Berberan-Santos, Mario (2012). Molecular Fluorescence: Principles and Applications. Wiley-VCHp. 64.

70. Lakowicz, Joseph R. (1999). Principles of Fluorescence Spectroscopy. Kluwer Academic/Plenum Publishers pp. 6-7

71. M. Biancalana, S. Koide, Biochim. Biophys. Acta 1804, 1405-1412 (2010)

72. M. Lindgren, P. Hammarstrom, FEBS J 277, 1380-1388 (2010)

73. M.R. Nilsson, Methods 34, 151-160 (2004)

74. Ellis, E. A. Methods Mol Biol 369, 97–106 (2007)

75. M.R. Krebs, L.A. Morozova-Roche, K. Daniel, C.V. Robinson, C.M. Dobson, Protein Sci. 13, 1933-1938 (2004)

76. J. Liu, C. Guo, Y. Yao, D. Lin, Biochimie 90, 1637-1646 (2008)

77. F. Meersman, L. Smeller and K. Heremans. Biophys J 82(5), 2635–44 (2002)

78. E. Pedone, S. Bartolucci, M. Rossi, F. M. Pierfederici, A. Scirè, T. Cacciamani, F. Tanfani. Biochem J 373(3), 875–83 (2003)

79. D. M. Byler and H. Susi. Biopolymers 25(3), 469–87 (1986)

80 J. L. Arrondo, A. Muga, J. Castresana, and F. M. Goni. Prog Biophys Mol Biol 59(1), 23–56 (1993)

81. A. Barth. Biochim Biophys Acta 1767(9), 1073–101 (2007)

82. S. Krimm and J. Bandekar, Adv Protein Chem 38, 181–364 (1986)

83. Y. N. Chirgadze and N. A. Nevskaya, Biopolymers 15(4), 607–25 (1976)

84. T. Nakagawa, S. Kishino, S. Itoh, M. Sugawara and K. Miyazaki. Br J Clin Pharmacol 56(6), 664–9 (2003)

85. A.Barth. Prog Biophys Mol Biol 74(3-5), 141–73 (2000)

86. A. Ausili, A. Scirè, E. Damiani, G. Zolese, E. Bertoli, F. Tanfani, Biochemistry (Moscow) 44, 15997-16006 (2005)

87. G. Anderle and R. Mendelsohn. Biophys J 52(1), 69–74 (1987)

88. D. Reinstadler, H. Fabian, J. Backmann and D. Naumann. Biochemistry 35(49), 15822–30 (1996)

89. D.M. Byler, H. Susi, Biopolymers 25, 469-487 (1986)

90. C. M. Chiu, Y. G Tsay, C. J. Chang and Lee, S. C. J Biol Chem 277(42), 39102–11 (2002)

91. O.B. Ptitsyn Trends Biochem Sci. 20(9), 376-9 (1995)

92. E. Pedone, S. Bartolucci, M. Rossi, F.M. Pierfederici, A. Scirè, T. Cacciamani, F. Tanfani Biochemical Journal 373(3), 875-883 (2003)

93. S. Paolini, F. Tanfani, C. Finia, E. Bertoli, P. Pelosic. Biochim Biophys Acta 1431(1), 179–188 (1999)

94. A. Marabotti, A. Scirè, M. Staiano, R. Crescenzo, V. Aurilia, F. Tanfani, S. D'Auria J. Proteome Res. 7 (12), 5221–5229 (2008)

95. H. Pages. Susi, S.N. Timasheff, L. Stevens. Journal of Biological Chemistry 242(23), 5460-5466 (1967)

96. M. Baldassarre, B. Maggiore, A. Scirè, F. Tanfani. Biochimie 118, 244-52 (2015)

97. A. L. Fink, S. Seshadri, R. Khurana and K. A Oberg. In nfrared Analysis of Peptides and Proteins, Singh, B. R., editor, volume 750 of ACS Symposium Series, 132–144. American Chemical Society, Washington, DC (1999)

98. J. Greenwald and R. Riek, Structure 18(10), 1244–60 (2010)

99. B. H. Toyama and J. S. Weissman. Annu Rev Biochem 80, 557–85 (2011)

100. R. Tycko, Q Rev Biophys 39(1), 1–55 (2006)

101. A. I. Sulatskaya, A. A. Maskevich, I. M Kuznetsova, V. N. Uversky, and K. K. Turoverov, PLoS One 5(10), 15385 (2010)

102. S. Kumar, J.B. Udgaonkar. Science 98(5), 639-656 (2010)

103. M.R.H. Krebs, Ludmilla A. Morozova-Roche, K. Daniel, C.V. Robinson, C.M. Dobson. Protein Sci. 13(7) 1933–1938 (2004)

104. K. Yamaguchia, S. Takahashia, T. Kawaib, H. Naikic, Y. Gotoa. Journal of Molecular Biology 352(4), 952–960 (2005)

105. A.K. Paravastu, I. Qahwash, R.D. Leapman, S.C. Meredith, R. Tycko. Proc Natl Acad Sci U S A. 106(18), 7443-8 (2009)

106. Ludmilla A. Morozova-Roche, J. Zurdo, A. Spencer, W. Noppe, V. Receveur, D. B. Archer, M. Joniau, C. M. Dobson. Journal of Structural Biology 130(2–3), 339-351 (2000)

107. Y. Miyamoto, S. Nishimura, K. Inoue, S. Shimamoto, T. Yoshida, A. Fukuhara, M. Yamada, Y. Urade, N. Yagi, T. Ohkubo, T. Inui. Journal of Structural Biology 169(2), 209–218 (2010)

108. A. Okuno, M. Kato, Y. Taniguchi. Biochem. et Biophysic Acta- Proteins and Proteomics 1764(8), 1407–1412 (2006)

109. S. Krimm, J. Bandekar. Advances in Protein Chemistry 38, 181–364 (1986)